

# JGR Solid Earth

## RESEARCH ARTICLE

10.1029/2023JB026577

### Key Points:

- Modern methods of deconvolution and migration technologies have significantly enhanced the value of a 40+ year seismic data set
- Reprocessing of legacy seismic data acquired at Hawaii provide the best examples we have of plate flexure caused by volcano loading
- Current difficulties in mounting new seismic experiments at sea require the reprocessing of legacy seismic data sets using modern methods

### Supporting Information:

Supporting Information may be found in the online version of this article.

### Correspondence to:

A. B. Watts,  
[tony.watts@earth.ox.ac.uk](mailto:tony.watts@earth.ox.ac.uk)

### Citation:

Cilli, P., Watts, A. B., Boston, B., & Shillington, D. J. (2023). Reprocessing of legacy seismic reflection profile data and its implications for plate flexure in the vicinity of the Hawaiian Islands. *Journal of Geophysical Research: Solid Earth*, 128, e2023JB026577. <https://doi.org/10.1029/2023JB026577>

Received 22 FEB 2023  
Accepted 18 AUG 2023

### Author Contributions:

**Conceptualization:** P. Cilli, A. B. Watts  
**Formal analysis:** P. Cilli, A. B. Watts, B. Boston, D. J. Shillington  
**Funding acquisition:** P. Cilli, A. B. Watts  
**Investigation:** P. Cilli, A. B. Watts  
**Methodology:** P. Cilli, A. B. Watts, B. Boston, D. J. Shillington  
**Project Administration:** P. Cilli, A. B. Watts  
**Software:** P. Cilli, A. B. Watts, B. Boston, D. J. Shillington  
**Supervision:** P. Cilli, A. B. Watts, B. Boston, D. J. Shillington

© 2023. The Authors.

This is an open access article under the terms of the [Creative Commons Attribution License](https://creativecommons.org/licenses/by/4.0/), which permits use, distribution and reproduction in any medium, provided the original work is properly cited.

# Reprocessing of Legacy Seismic Reflection Profile Data and Its Implications for Plate Flexure in the Vicinity of the Hawaiian Islands

P. Cilli<sup>1</sup> , A. B. Watts<sup>1</sup> , B. Boston<sup>2,3</sup> , and D. J. Shillington<sup>4</sup> 

<sup>1</sup>Department of Earth Sciences, University of Oxford, Oxford, UK, <sup>2</sup>Lamont Doherty Earth Observatory of Columbia University, Palisades, NY, USA, <sup>3</sup>Now at Department of Geosciences, Auburn University, Auburn, AL, USA, <sup>4</sup>School of Earth and Sustainability, Northern Arizona University, Flagstaff, AZ, USA

**Abstract** During 1975–1988, an academic research ship, R/V *Robert D. Conrad*, acquired more than 150,000-line-km of multichannel seismic reflection profile data from each of the world's main ocean basins and their margins. This extensive legacy seismic data set, which involved both single ship and two-ship data acquisition, has been widely used by the marine geoscience community. We report on our experience in reprocessing seismic reflection profile data acquired during *Conrad* cruise RC2308 to the Hawaiian Islands region in August/September 1982. We show that the application of modern, industry standard processing techniques, including filtering, de-bubble, deconvolution, and migration, can significantly enhance 40+ year old legacy seismic reflection profile data. The reprocessed data reveals more precisely, and with much less scatter, the flexure of Cretaceous Pacific oceanic crust caused by the Pliocene-Recent volcanic loads that comprise the Hawaiian Islands. A comparison of observed picks of top oceanic crust which has been corrected for the Hawaiian swell and the Molokai Fracture Zone with the calculations of a simple 3-dimensional elastic plate (flexure) model reveals a best fit elastic plate thickness of the lithosphere,  $T_e$ , of 26.7 km, an average infill density of 2,701 kg m<sup>-3</sup>, and a Root Mean Square difference between observations and calculations of 305 m. Tests show these results depend weakly on the load density assumed and that the average infill density is close to what would be predicted from an arithmetic average of the flanking moat infill density and the infill density that immediately underlies the volcanic edifice.

**Plain Language Summary** The mid-1970s to mid-1980s saw a rapid increase in the acquisition of marine seismic reflection profile data by academic research vessels using large airgun arrays and long multichannel streamers. The data have provided some of the best images we have of the structure of mid-ocean ridges, transform faults and fracture zones, and deep-sea trenches; however, the processing of these data was rudimentary in comparison to modern standards. We show here how reprocessing of seismic reflection profile data acquired some 40+ years ago in the vicinity of the Hawaiian Islands that utilize modern methods of filtering, deconvolution, and migration technologies have significantly improved imaging of the top and bottom of oceanic crust, reducing the scatter in reflector depths from a legacy data set by almost a factor of two. This, in turn, has led to improved resolution of the large-scale deformation caused by the individual volcano loads that comprise the Hawaiian Islands and, since the ages of these loads and the ocean floor on which these loads have been emplaced are known, to a better understanding of the stress state, strength, and rheological properties of Earth's tectonic plates.

## 1. Introduction

Seismic reflection profiling is one of the principal methods with which we can image the deep structure of Earth's crust and upper mantle. During 1975–1988, the research vessel *Robert D. Conrad*, owned by the US Navy and operated by the Lamont-Doherty Geological Observatory of Columbia University, acquired more than 150,000-line km of marine geophysical data, including MultiChannel Seismic (MCS) reflection profile data, during 31 approximately 30-day-long cruises to the Atlantic, Indian, and Pacific Ocean basins and their margins. This extensive legacy seismic data set, which involved both single and two-ship experiments, has been widely used by the marine geoscience community to determine sediment thickness in the deep oceans (e.g., Sheridan et al., 1978), to image the velocity structure and Moho of oceanic crust at mid-ocean ridges (e.g., Vera & Diebold, 1994), fracture zones (e.g., Minshull et al., 1991) and active (e.g., Lewis & Hayes, 1989) and passive continental margins (e.g.,

**Validation:** P. Cilli, A. B. Watts, B. Boston, D. J. Shillington  
**Writing – original draft:** P. Cilli, A. B. Watts  
**Writing – review & editing:** P. Cilli, A. B. Watts, B. Boston, D. J. Shillington

Mutter et al., 1984), and to constrain processes of oceanic crustal accretion (e.g., Detrick et al., 1987) and subduction (e.g., Bangs & Cande, 1997) and models for the thermal and mechanical evolution of oceanic lithosphere (e.g., Watts et al., 1985; Wessel, 1993) and the rheological laws that describe brittle deformation and ductile flow at lithospheric conditions (e.g., Zhong & Watts, 2013).

The *Conrad* MCS data were usually processed at Lamont-Doherty Geological Observatory using “in-house” software within a few years of its acquisition, but with few exceptions have not been reprocessed since then. Although the data set was acquired with the latest technology available to academia at the time, many cruises lacked a near-field hydrophone and tuned air-gun arrays. This led to significant issues in the processing, and imaging, for example, in removal of bubble pulse reverberations. Furthermore, processing was based on “in-house” computer software that focussed on de-noise, filtering, and velocity analysis, which was simple by today's standards. Since the late 1980s, however, there has been considerable progress in the development of software for the processing of seismic reflection profile data. Today, industry-standard software is widely available in academia which utilizes an array of sophisticated processing and imaging algorithms including de-noise, de-bubble, deconvolution, and many different time and depth migration techniques (e.g., Yilmaz, 2001).

The purpose of this paper is to present the results of reprocessing of the *Conrad* MCS data acquired more than 40 years ago during a single- and two-ship seismic experiment in the vicinity of the Hawaiian Islands, central Pacific Ocean. We show that reprocessing using modern techniques can considerably enhance a legacy seismic data set to the extent that it improves the signal-to-noise ratio of the data and improves geological interpretation. The results of our work have implications for the many other seismic data sets acquired on *Conrad*. In particular, undertaking reanalysis of these legacy data sets with modern methods is important given the complexities today of acquiring deep seismic data due, for example, to the establishment of marine conservation areas, ambiguities in offshore territorial claims, and the possible effect of the seismic source on marine mammals and their habitats. The results of this reprocessing also enable new insights into the crustal structure of the hotspot generated Hawaiian Ridge and the oceanic lithosphere on which it was constructed.

## 2. *Conrad* RC2308 Cruise

During August/September 1982, the US Navy owned, and Lamont-Doherty Geological Observatory of Columbia University operated research vessel R/V *Robert D. Conrad*, acquired approximately 5484-line km of MCS data (Buhl & Watts, 1982) along three transects which intersected the Hawaiian Ridge between the islands of Oahu and Molokai and Oahu and Kauai (Figure 1). The *Conrad* was equipped during the experiment with a  $2 \times 1,000$  (16.4 l) and  $1 \times 466$  cu. in. (7.6 l) Bolt air gun array, a Seismic Engineering 3.6-km-long analog hydrophone streamer, a Bell Aerospace BGM-3 air-sea gravimeter and a Loran C and Magnavox satellite navigation system.

The orientation of the three transects, shown in Figure 1, was designed to cross the calculated flexural depression, and flanking moats and bulges at a high angle. The “central” transect (i.e., labeled Lines 301 and 314 in Figure 1) was a two-ship experiment that involved *Conrad* and a second ship, R/V *Kana Keoki* from the University of Hawaii which was equipped with a source array comprised of  $1 \times 1,000$  and  $2 \times 466$  cu. in. airguns. During the experiment, the lead ship, *Kana Keoki*, was separated from *Conrad* by a constant offset which was continuously monitored using a Miniranger/Raydist system (Figure 2). Constant bearings of the *Kana Keoki* were recorded on *Conrad*'s Bridge to ensure the two ships maintained a constant offset. *Conrad* and *Kana Keoki* shot on alternate half minutes into *Conrad*'s streamer.

“Constant Offset Profiles” (COPs) were acquired to the south and north of Oahu along the central transect. The southern part of the central transect was made up of a southbound Constant Offset Profile (COP) A at an offset of 3.6 km and northbound COPs B, C, and D (Figure 3) at an offset of 16 km. The northern part of the central transect was made up of a northbound COP F at an offset of 3.6 km and southbound COPs G, H, and I (Figure 4) at an offset of 16 km. The 16 km offset was selected at sea based on disposable sonobuoy data (open circles in Figure 1), which showed strong, well-defined, sub-critical reflections at this range. The reflection data acquired with this novel two-ship configuration resulted in the equivalent of data acquired from a single ship with a long streamer and high receiver density.

In between the northbound COPs B, C, and D south of Oahu and southbound COPs G, H, and I north of Oahu, Expanding Spread Profile (ESP) seismic refraction data were acquired during which the two ships separated in opposite directions from a mid-point (Figures 3 and 4) to an end point about 60 km from the mid-point. At the end

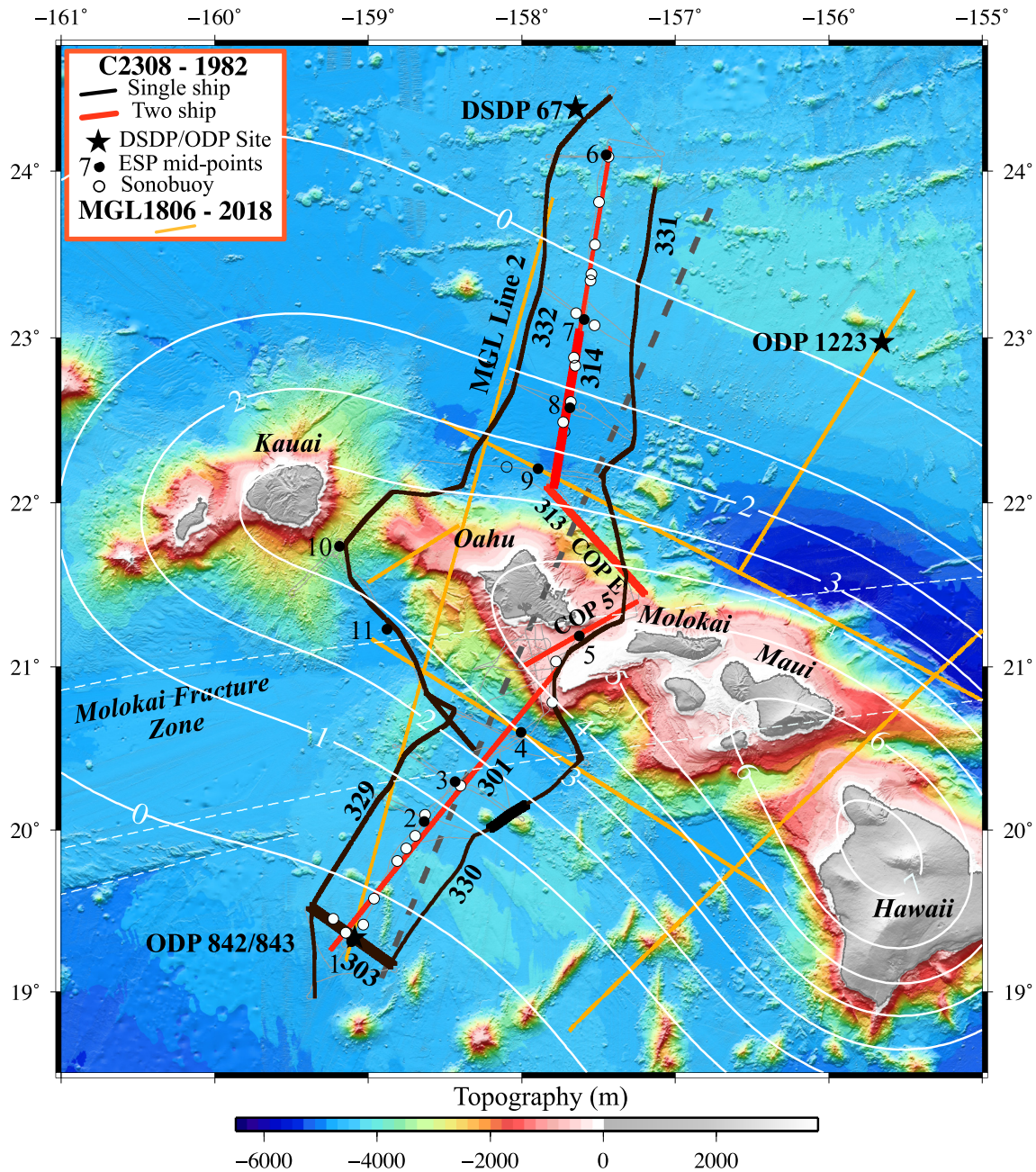


**Figure 1.** Location map of the Hawaiian Islands region showing the Multi-Channel Seismic (MCS) reflection profiles acquired during R/V *Robert D. Conrad* Cruise RC2308 (solid black and red lines) together with the newly acquired MCS data during R/V *Marcus G. Langseth* cruise MGL1806 (solid orange lines). Thick lines locate the segments of MCS data shown along Lines 303, 314, 313 Constant Offset Profile E and 330 in Figures 7–10, respectively. Filled black circles (with number) show Expanding Spread Profile (ESP) mid-points. Filled white circles show sonobuoys deployed during the experiment that recorded refractions. Dashed gray line shows the profile along which the velocity data acquired at ESP mid-points was projected. Bathymetry is based on a  $1 \times 1$  min grid of GEBCO single beam echo-sounder and multibeam (swath) data plus NASA Shuttle Radar Topography (SRTM 2020) data. Thin dashed white lines locate the strands of the Molokai Fracture Zone as digitized by Matthews et al. (2011). Solid white lines show the calculated flexure of the lithosphere (contour interval = 1 km) due to the surface load of the Hawaiian Islands, assuming an effective elastic thickness of the lithosphere,  $T_e$ , of 30 km.

points each ship turned on a reciprocal course and approached each other. During the “outgoing” segment *Kana Keoki* fired its airguns at 1 min interval and *Conrad* received while during the “incoming” segment *Conrad* fired its airguns at 1 min interval with every 10 minute missing and *Kana Keoki* fired its explosive charges at 10-min intervals. This ESP data, together with sonobuoy data, provided the necessary  $P$  wave velocity data for converting the recorded MCS reflection profile data from travel time to depth.

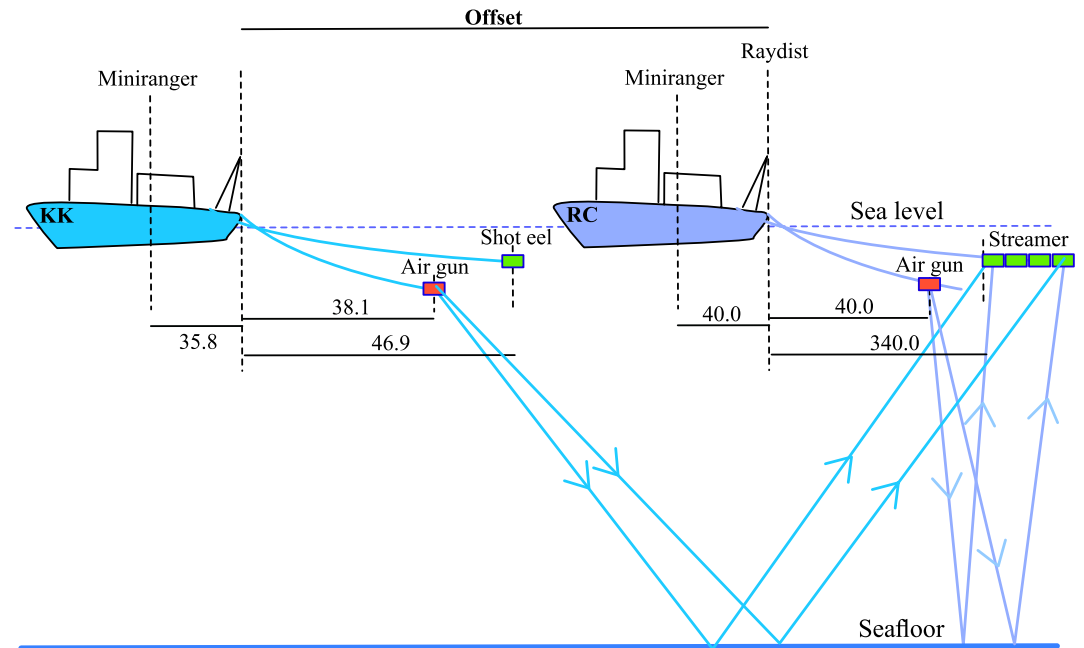


**Figure 2.** Schematic diagram showing the geometry of data acquisition during the two-ship experiment. Also shown is the raypath of a seafloor reflected arrival generated by each ship firing alternately into the head and tail active section of Conrad's streamer.

The western and eastern transects (i.e., Lines 329, 330, 331, and 332 in Figure 1) were a single ship experiment in which *Conrad* acquired MCS data along lines connecting the ESP end points. During this part of the experiment *Conrad* shot to its 3.6-km-long streamer at 20 s intervals with a recording length of 12 s.

Data from the two-ship and single ship experiments were recorded on each of the 48 channels of *Conrad*'s streamer which, in turn, were logged on a Texas Instrument DFS IV on 1600 DPI 9-track tape with a 4- or 8-ms sampling rate and recording lengths of 20, 39, and 12 s for the COP, ESP, and CDP part of the experiment respectively. There were a total of ~43,250 shots, resulting in 867 9-track tapes and approximately 20-GB of digital data.

### 3. Seismic Data Reprocessing

In 2016 Lamont-Doherty Earth Observatory entered into an agreement with ION Geophysical in Houston, Texas to convert all the 9-track MCS data tapes acquired on *Conrad* to a standard SEG-Y format (S. Carbotte, pers. comm). The digitized data for the *Conrad* RC2308 cruise was released early by ION so that it could be used for ship track planning for the R/V *Marcus G. Langseth* MGL1806 seismic reflection and refraction cruise (Boston et al., 2019; Dunn et al., 2019) which took place during April/June 2018.

The first step in the reprocessing was to generate the navigation data and merge it with the digitized legacy gathers. Using the navigation data recorded on the *Conrad* and *Kana Keoki*, as well as the idealized acquisition geometry shown in Figure 2, we created a nominal survey geometry for all seismic lines, including an estimated X-Y pair for all shots, receivers, and CMP locations.

The northern and southern parts of the central transect (Figures 3 and 4) consisted of eight COPs and so were processed as two separate composite lines: Line 301 south of Oahu and Line 314 north of Oahu. The processing flow for each line consisted of loading the four individual SEG-Y files into the Shearwater Geoservices Ltd *Reveal* processing software and performing trace edits and quality control. The four seismic volumes were then merged into one for the remainder of the processing. At this point, source and receiver depth headers were assigned and the data was gridded to the nominal line geometry, calculating midpoint locations from the ship's navigation for each source-receiver pair. The midpoints were then projected onto a line or curve for reprocessing.

Pre-processing involved a 5 Hz low-cut filter, F-X swell noise removal in the shot then channel domain, self-consistent amplitude corrections, and Surface-Related Multiple Attenuation (SRMA) (Figure 5). The subsequent deconvolution process was focussed primarily on bubble pulse removal due to the strong bubble pulse present in the source signature.

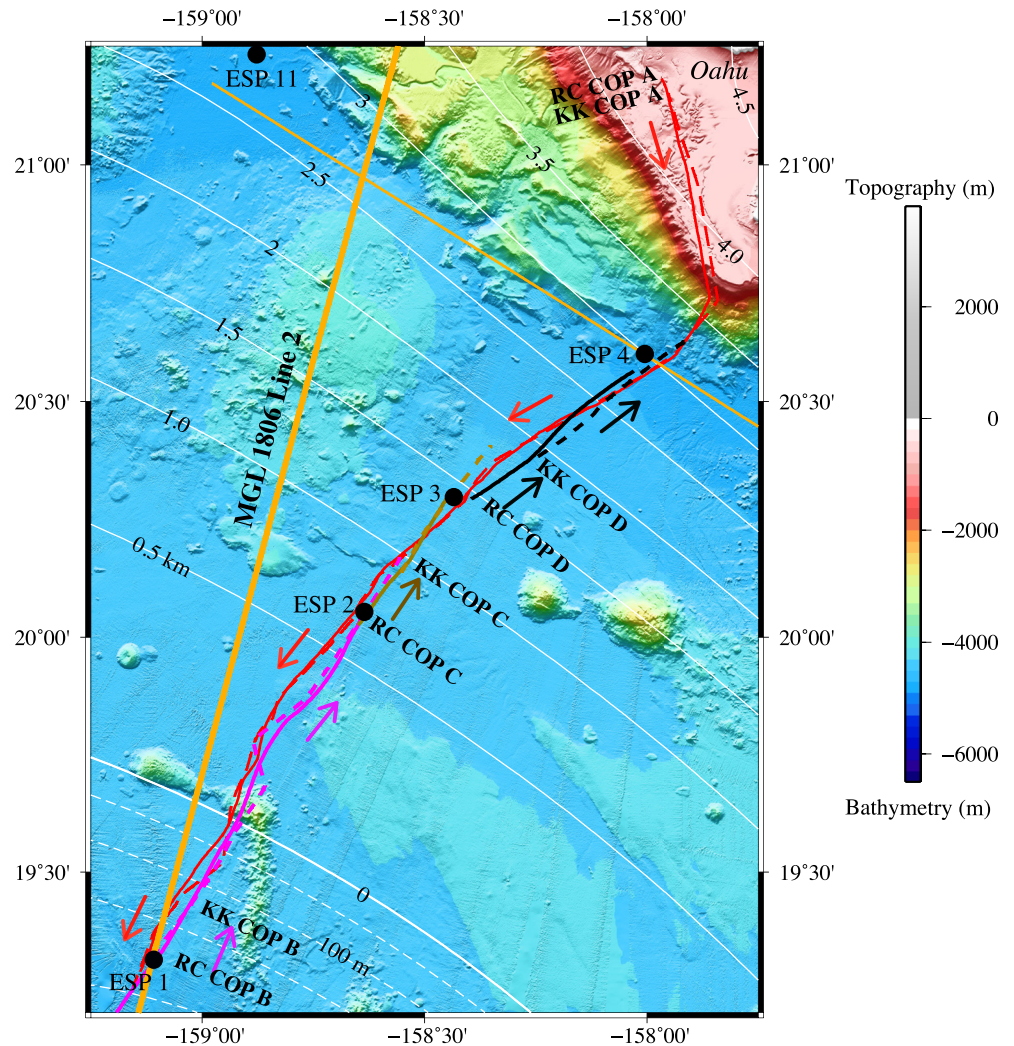


**Figure 3.** The two-ship experiment south of Oahu which comprised an “outgoing” (i.e., southbound) Constant Offset Profile (COP) A (red solid line) at a ship separation of 3.6 km and “ingoing” (i.e., northbound) COPs B (purple solid line), C (brown solid line), and D (black solid line) at a ship separation of 16 km. Filled black circles show Expanding Spread Profile mid-points. RC = Robert D. Conrad (solid lines). KK = Kana Keoki (dashed lines). White solid lines show the flexural depression at 0.5 km interval for the same value of the elastic thickness as used in Figure 1. White dashed lines show the flexural bulge at 50 m interval.

Velocity models were created for processing and imaging after preliminary pre-processing (low-cut filter and swell noise reduction) was performed. The center point for ESP 1–9 *P* wave velocities were located along the central transect (Figure 1, red lines) while ESPs 10 and 11 were located on the western transect (Figure 1, Line 332). Therefore, the velocity model for the central and eastern transects (Figure 1, Lines 301, 314, COP 5, COPE, 330, and 331) was built using velocities from only ESPs 1–9. The original ESP digital seismic data was unavailable for reinterpretation, so rather than re-deriving ESP velocities from the seismic data, we used the original interpretations reported in the literature by Watts et al. (1985), ten Brink (1986), Brocher and ten Brink (1987), ten Brink and Brocher (1987), and Lindwall (1988a, 1988b).

To generate a velocity model that spanned the central and eastern transects, the midpoint locations of ESPs 1–9 were projected onto a central line passing through Oahu (Figure 1, dashed gray line). We chose this line because it is approximately perpendicular to the local trend of the Hawaiian Ridge and was used to project the RC2308 gravity, bathymetry, and legacy interpretations (referred to as “picks” in this paper) of the seismic data in Watts et al. (1985) and Watts and ten Brink (1989). All the ESP mid-point *P* wave velocities were available as a function of depth below the seafloor and so were resampled with linear interpolation onto a regular, finely spaced depth grid before smoothing

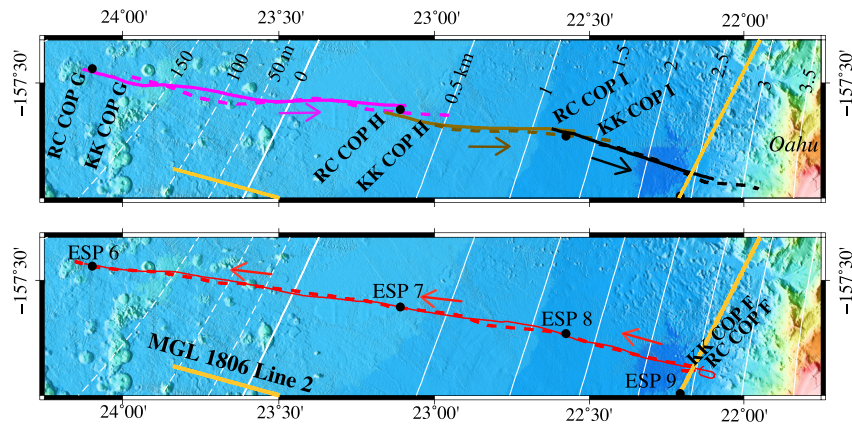


**Figure 4.** The two-ship experiment north of Oahu which comprised an “outgoing” (i.e., northbound) Constant Offset Profile (COP) F at a ship separation of 3.6 km and “ingoing” (i.e., southbound) COPs G, H, and I at a ship separation of 16 km. White lines are as defined in Figure 3.

was applied. After this, interpolation between the depth-gridded velocity trends was performed along the line of projection, creating a 2D velocity profile. This velocity profile was then projected outwards onto the central and eastern transects, producing a velocity model for each profile which had vertical dimension depth sub-seafloor (Figure 6).

To finalize the velocity model, all seismic data were migrated with a constant water velocity of 1,500 m/s and water-bottom horizons were picked on the resultant images. The velocity models were then translated to beneath these water-bottom horizons and the water column flooded with a water velocity. In some cases, small seamounts were not considered in picking these water-bottom horizons to avoid artificial velocity pull-ups, as the main priority of this study was to image the top and bottom of oceanic crust in depth. The velocity profile for the western transect was created in the same way as the central and eastern transects, however ESPs 10 and 11 were used instead of ESP 5 in the model building process.

A combination of Kirchhoff Pre-stack time migration and angle stacking was used to create the final seismic images, whereby migration to 4 km offset with an aperture of 6 km was used into the oceanic crust, before

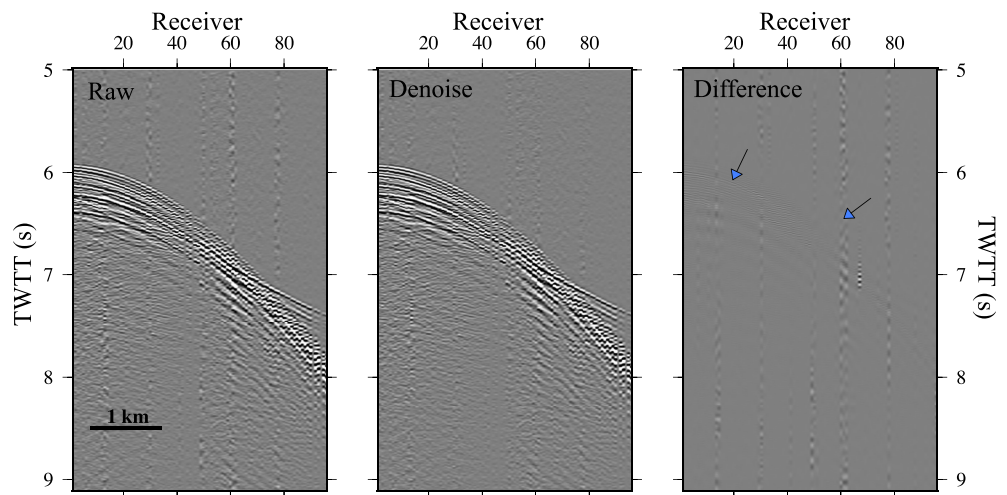


**Figure 5.** An example of a conservative denoise (the term “denoise” is used here and elsewhere in the text to collectively describe basic processing steps such as trace edits, bandpass filtering, and FX swell noise removal in the shot and channel domains) applied to a “shot” gather (FFID 2499) from Conrad and Kana Keoki alternately shooting into Conrad’s streamer along Line 301 in the flexural moat south of Oahu, showing before (left) and after (middle) denoise as well as their difference (right). Pre-processing shown includes low-cut filtering, F-X swell removal in shot and channel domain, self-consistent amplitude correction, and Surface-Related Multiple Attenuation (water bottom multiple not visible). Accordingly, some low frequency bubble noise (left arrow) is removed as well as swell and other noise (right arrow). The gather shows reflections from the seafloor and from sediments in the sub-seafloor and a refraction emerging at offsets of ~2.2 km and greater.

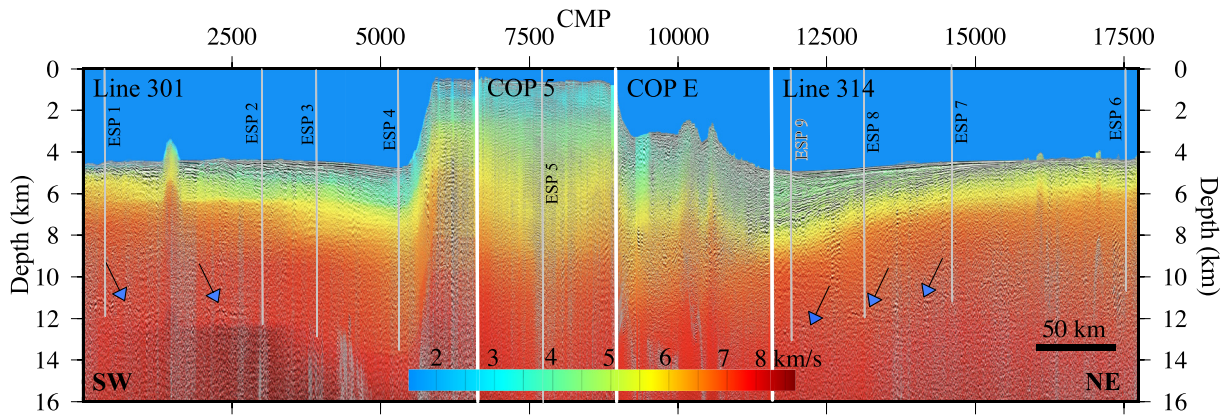


**Figure 6.** *P*-wave velocity versus depth model based on data from Expanding Spread Profiles (ESPs) 1–9 (Figures 3 and 4) superimposed on reprocessed Lines 301, Constant Offset Profile (COP) 5, COP E, and 314 which intersected the Hawaiian Ridge between Oahu and Molokai (Figure 1). The velocity model was used to convert the two-way travel time seismic image to depth. Thin white lines locate the ESPs. Thick white lines separate reprocessed Lines COP 5 and COP E from composite Lines 301 and 314. Blue arrows delineate the reflection Moho.

merging with a stack from above the Moho to the end of the trace. This is because the structures visible above the oceanic crust were imaged best with migration while the Moho was imaged best by stacking, presumably because of the nature and strength of the noise at the depth of the Moho.

After this merging, post-stack processing was performed including gain enhancement in the frequency domain, F-K coherency filtering and a depth-dependent low-pass filter. The final step in the processing flow was converting the seismic images to depth using the respective ESP-derived velocity models.

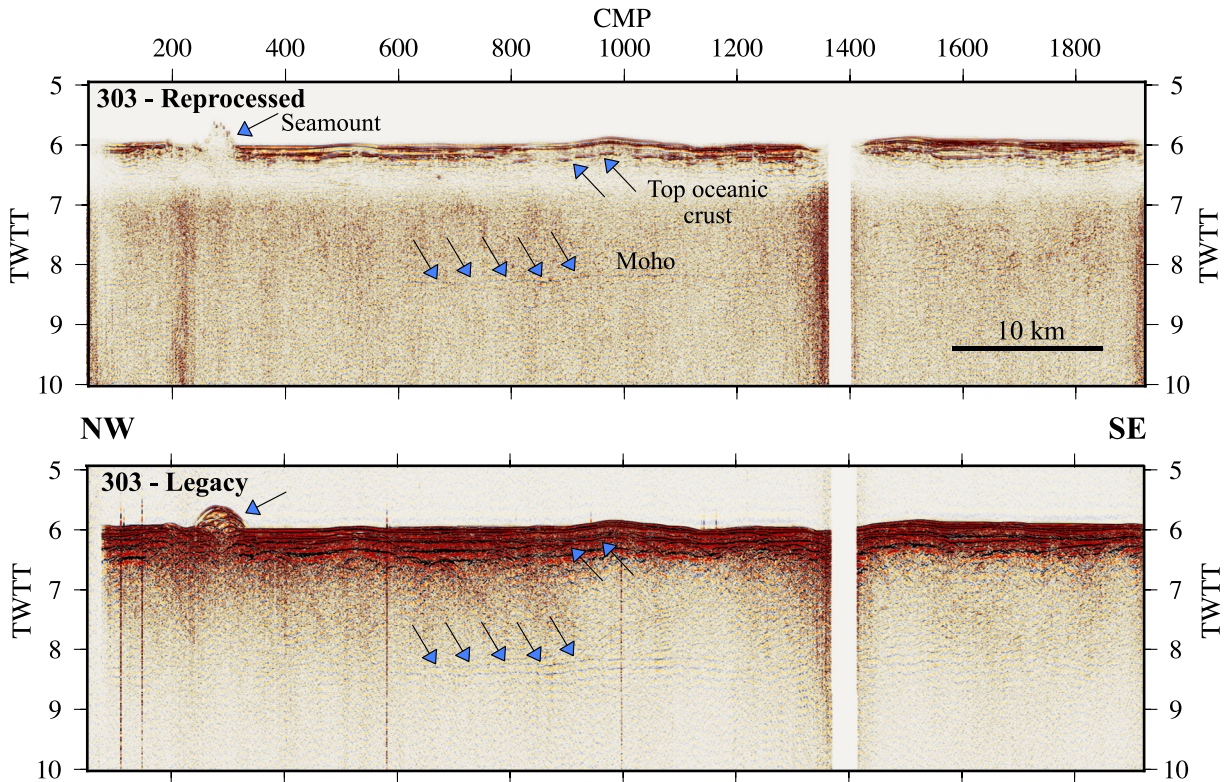


**Figure 7.** Reprocessed (top) and legacy (bottom) seismic images of Line 303 of the flexural bulge southwest of Oahu (Figure 1). Improvements from reprocessing include a sharpened Moho, reduced ringing, and better-imaged sediment and top oceanic crust (blue filled arrows). The ringing below the top of oceanic crust (upper arrows) and Moho (lower arrows) in the legacy data is due to the bubble pulse, which was not removed during processing due to a difference in available technology. The improved imaging of the seamount (left-hand arrow) in the reprocessed data demonstrates the possible gains in imaging steep structures from migration.

We applied the processing flow outlined above to all lines with the following exceptions: COP E and COP 5 had demultiple by parabolic radon applied after SRMA. Lines 331 and 332 had an additional gap deconvolution applied to supplement their debubble. The depth conversion velocity for COP E was clipped to a maximum value of  $5.2 \text{ km s}^{-1}$  because we observed velocities that were too fast over what we considered to be mostly extrusive landslide material on the north flank of Oahu. The choice of  $5.2 \text{ km s}^{-1}$  was largely based on shallow igneous crustal velocities derived from a preliminary interpretation of Ocean Bottom Seismometer (OBS) data along *Langseth* Line 2 which also crossed the north flank of Oahu (Boston et al., 2019). In addition, Line 303, on the bulge southwest of Oahu, was converted to depth for comparison with IODP drill site horizons using an ESP velocity where all velocities greater than  $2.5 \text{ km s}^{-1}$  shallower than 5 km depth were set to  $2.5 \text{ km s}^{-1}$ . This allowed us to more accurately account for the varying depth of top of oceanic crust along the line while enabling the well tie.

Due to the lack of available field data for Line 330, we reprocessed the Line 330 legacy stack that is available from the Marine Geoscience Data System (MGDS) online data repository (<https://www.marine-geo.org/index.php>). The simple post-stack reprocessing flow for this line was merging the online navigation with the seismic, applying static corrections, applying a low-cut then depth-dependent low-pass filter, followed by depth-dependent gap deconvolution. Finally, we performed post-stack Kirchhoff time migration then depth conversion using the ESP  $P$  wave velocity model.

Figure 7 shows both the legacy and reprocessed seismic images of Line 303 from the flexural bulge southwest of Oahu, where sedimentary structures and Moho are clearer and have less ringing in the reprocessed data. This improvement is largely due to effective bubble pulse removal and filtering. Steeply dipping reflectors (e.g., on or near the sea floor) are also imaged better due to pre-stack migration. Figure 8 shows the same types of improvements on Line 314, which crosses the northern moat of Oahu. A spectrum plot is also shown in Figure 8, highlighting the improvements in frequency content due to debubbling, denoise, and filtering. These improvements include broadening the spectrum, removing the low frequency energy surge indicative of the bubble pulse, and generally balancing the spectrum to bring out higher frequencies.

Figure 9, which shows COP E (Line 313, Figure 1), reveals the same general improvements as Figures 7 and 8. In particular, we improve imaging of a reflector at  $\sim 6.5\text{--}7.5 \text{ s}$  on the northeast flank of Oahu that we interpret as a décollement surface that separates the volcanic edifice from the top of the oceanic crust, similar to one identified by Morgan et al. (2003) from MCS data acquired on R/V *Ewing* on the south flank of Kilauea. The décollement connects directly to the base of the moat sediment and top of oceanic crust at approximately 7.5 s on CMP 2420. We note that migration noise from residual water bottom multiple is still present in the reprocessed data (approximately CMP 1500) and should not be interpreted as geological structure. Interestingly, COP E was not previously published nor used in prior flexure calculations. A structural interpretation of a depth converted representation of COP E Line 313 is shown in Figure S1 in Supporting Information S1.

Figure 10 shows improved imaging of Line 330, which crosses the flexural moat southwest of Oahu, due to post-stack processing, as most of the line's field data was not available for pre-stack reprocessing. We focus on two small seamounts in the moat that highlight the benefits of post-stack time migration, including improved imaging of both sub-vertical structures and diffractors.

#### 4. Interpretation

The depth converted reprocessed RC2308 seismic data, which are available from Cilli et al. (2023), were subsequently loaded into the *Paradigm* seismic processing and interpretation software at Lamont-Doherty Earth Observatory, where we “picked” the top of oceanic basement, Moho, and a possible décollement surface separating the volcanic edifice from the top of oceanic crust. Picks of the reprocessed data were then verified by Ocean Drilling Project (ODP) drilling data at Site 843A/B and compared with picks on intersecting MGL1806 Line 2 (Figure 1), and with the predictions of the structure of pre-existing Cretaceous Normal Polarity Pacific oceanic crust and simple elastic plate models of volcano loading in the vicinity of the Hawaiian Islands. Examples of the picks of top oceanic crust and Moho along the three long transect profiles (Figure 1) are shown in Figures S2–S4 in Supporting Information S1.

Figure 11 shows a close agreement between the depth of the sediment/basalt contact at ODP Sites 843A and 843B (Shipboard Scientific Party, 1992) and the top of oceanic basement picks on RC2308 Line 303. The sediment/basalt contact at  $\sim 242 \text{ m}$  and samples of basalt recovered at depths of  $\sim 262$ ,  $\sim 288$ ,  $\sim 297$ , and  $\sim 304 \text{ m}$  confirm that our picks correspond to the top of oceanic crust and not a reverberant layer caused, for example,



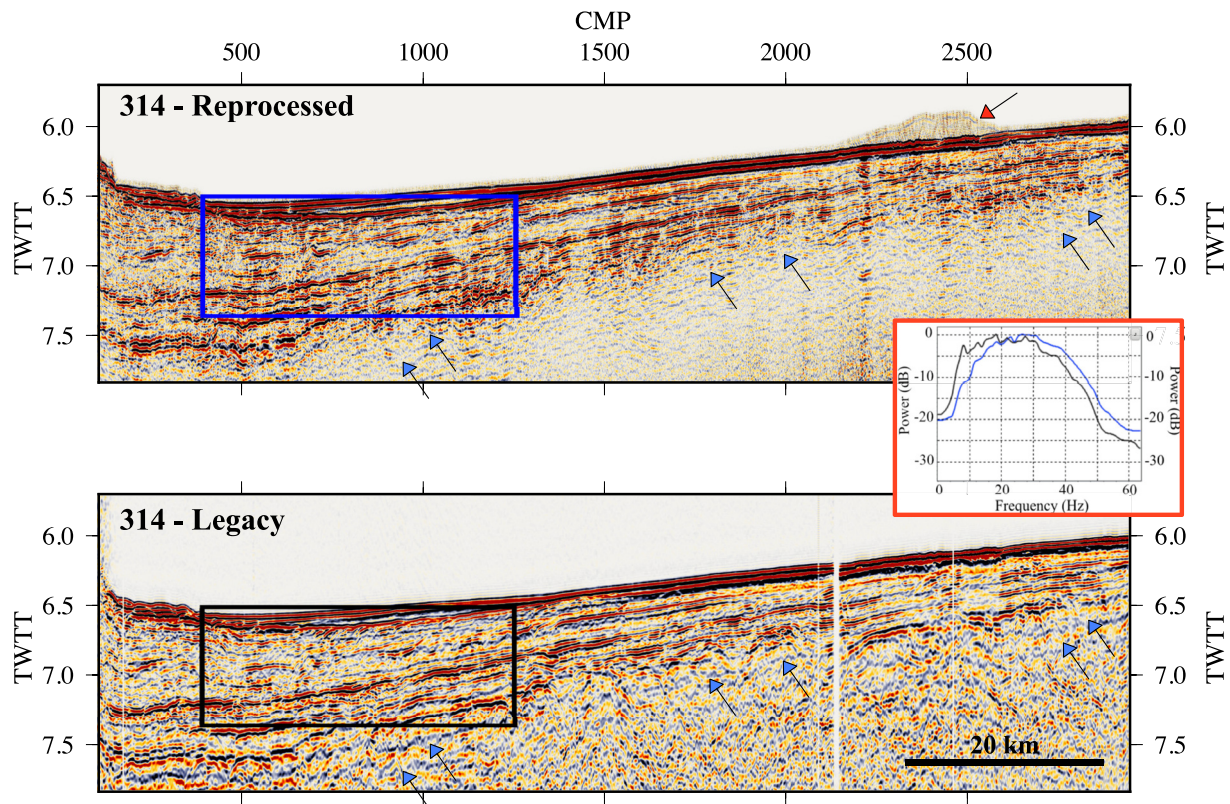


**Figure 8.** Reprocessed (top) and legacy (bottom) seismic images of Line 314 of the flexural moat northeast of Oahu (Figure 1). Improvements from reprocessing include enhanced frequency content, reduced ringing, better-imaged sediment with more continuous strata, and a more clearly defined basement reflector. Inset shows a power spectrum of reflectors from the box region. The reduction and smoothing of the frequency spectrum between approximately 0 and 20 Hz is characteristic of an effective debubble, which corresponds to less high-amplitude ringing in the seismic data, seen dramatically in the lower left, middle, and right side of the legacy data. The top of a seamount is imaged in the reprocessed data (red filled arrow) as, unlike in the legacy data, the reprocessed data is a composite data set containing recordings from Lines 314, 317, 320, and 323; only one of which transited a seamount.

by younger deep-water volcanism. Sediment thickness varies little along the line, as expected for its orientation sub-parallel to the trend of the flexural bulge and moat southwest of Oahu. Sites 843A and 843B penetrated an upper yellow-brown clay layer which overlies a chert and nannofossil limestone layer and there is good evidence in the reprocessed data of a change in seismic facies at the depth of  $\sim 122$  m (Orange horizontal bar in Figure 11) that separates these two lithostratigraphic units.

Figure 12 compares the legacy and reprocessed picks along a line of projection centered on the southwest flank of Oahu: between Waianae volcano in the west and Koolau volcano in the east (dashed gray line, Figure 1). The figure shows the picks of reprocessed data to be significantly smoother and less scattered than the original picks of legacy data, which we attribute to the application of modern processing techniques and to a greater accuracy of the digitization of reflectors (picking was carried out digitally in the *Paradigm* software rather than manually on a light-table). Northeast of Oahu, the reprocessed picks reveal a remarkably smooth flexure of the top of oceanic crust that extends for distances of  $\sim 250$  km from the flank of the volcanic edifice and to depths beneath it of up to  $\sim 4$  km. Moho is not as well resolved, but the reprocessed data suggest that it too is flexed over a similar distance and depth.

According to previous interpretations of legacy seismic reflection and ESP 5 velocity data (e.g., ten Brink & Brocher, 1987; Watts et al., 1985) and receiver function data (e.g., Leahy & Park, 2005; Leahy et al., 2010), flexed Pacific oceanic crust between Oahu and Molokai may be underplated by magmatic material, the upper and lower surfaces of which are at depths of  $\sim 14$  and  $\sim 18$  km respectively. The underplated material is intermediate in  $P$  wave velocity and density between lower crust and mantle and has been interpreted to represent melt that had ponded beneath flexed crust and subsequently cooled (e.g., Watts & ten Brink, 1989). However, we have found no evidence in the reprocessed reflection data for such an underplate. This is not to imply that the oceanic crust

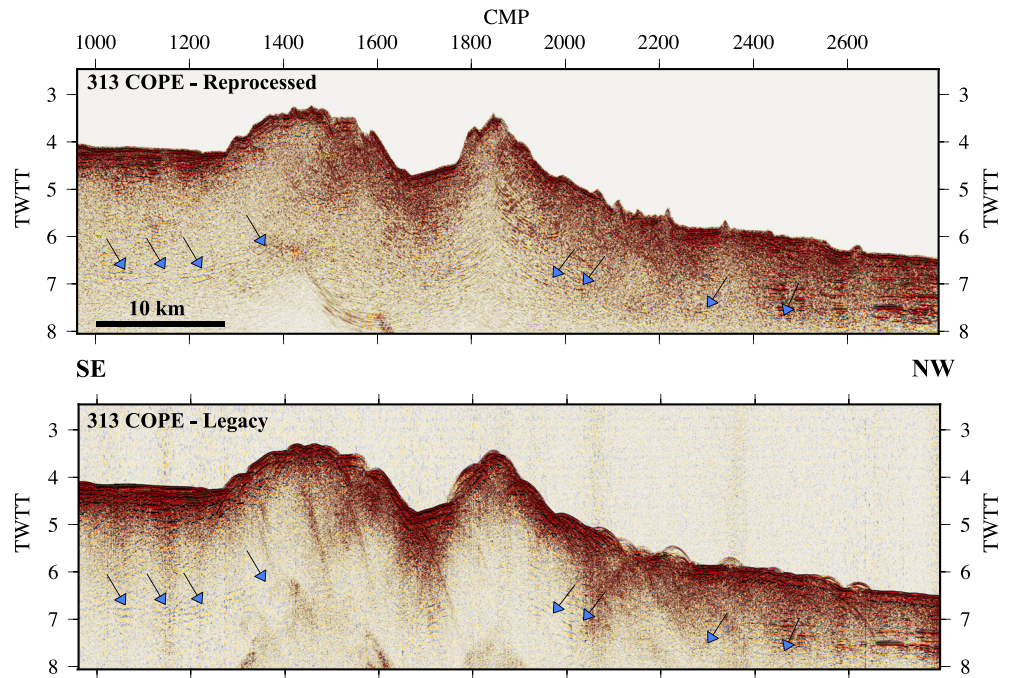


**Figure 9.** Reprocessed (top) and legacy (bottom) seismic images of Line 313 Constant Offset Profile E which crossed the northeast flank of Oahu (Figure 1). The flexural moat is just visible on the northwest end of the line. Improvements from reprocessing include a more visible and sharpened décollement reflector, reduced ringing, and better-imaged sediment and bathymetry. A mid-slope sedimentary basin is imaged in the reprocessed data between CMPs 1600 and 1800 and the improvement on seamount imaging along the line is notable. The moat sediment is visible on the lower right-hand side, where the base of this (i.e., the top of oceanic crust) becomes what we interpret as the décollement reflector, highlighted by blue arrows. Migration noise from residual water bottom multiple is seen in the reprocessed seismic at CMP 1500, TWT 7.5 s.

between Oahu and Molokai is not underplated, but evidence needs to be established, not from reflection data, but from deep seismic refraction data. Indeed, Lindwall (1988b) did not find any evidence of an intermediate velocity and density layer from his modeling of ESP 5, preferring instead Moho at a depth of  $\sim 14$  km. The best evidence, however, will likely come from closely spaced OBS data such as that deployed along Line 2 during the *Langseth* cruise since these data have the most potential to determine the lateral changes in  $P$  wave velocities associated with such an underplate model (e.g., Dunn et al., 2019).

Southwest of Oahu, the top of oceanic crust is not as smooth as to the northeast and appears to be offset in the region of the Molokai Fracture Zone (MFZ) upon which the Hawaiian Ridge has been emplaced. The MFZ is clearly visible in the satellite-derived gravity anomaly field (e.g., Matthews et al., 2011; Sandwell et al., 2019), and these data show its southern offset intersects the line of projection approximately between ESP 2 and ESP4 mid-points while its northern offset extends toward a region between COP E and its intersection with Line 331. The gray shade in Figure 12 delineates the approximate extent of the two main strands of the MFZ along the line of projection where there is evidence for a shallowing of the top of oceanic crust by up to a few hundreds of meters and, possibly, a thinning of the oceanic crust along both the western and eastern transects.

## 5. Flexure Modeling

The picks of the top of oceanic crust from the RC2308 legacy and reprocessed data sets have been used to re-assess the surfaces of flexure associated with the loading of the Hawaiian volcanoes and the long-term mechanical properties of the Pacific oceanic lithosphere. The first step was to estimate the elastic thickness,  $T_e$ , and the average infill density using a grid search algorithm. Specifically, the observed picks are compared to the predictions of a simple 3D elastic plate model in which the load is defined from a  $1 \times 1$  min GEBCO + SRTM 2020 bathymetric grid and a Young's modulus of 100 GPa, Poisson's ratio of 0.25, a uniform load density of  $2,737 \text{ kg m}^{-3}$ , a uniform density of the material that underlies the plate of  $3,330 \text{ kg m}^{-3}$  and a range of possible uniform elastic thickness (0–50 km) and average infill density values ( $2,100$ – $2,800 \text{ kg m}^{-3}$ ) are assumed. After

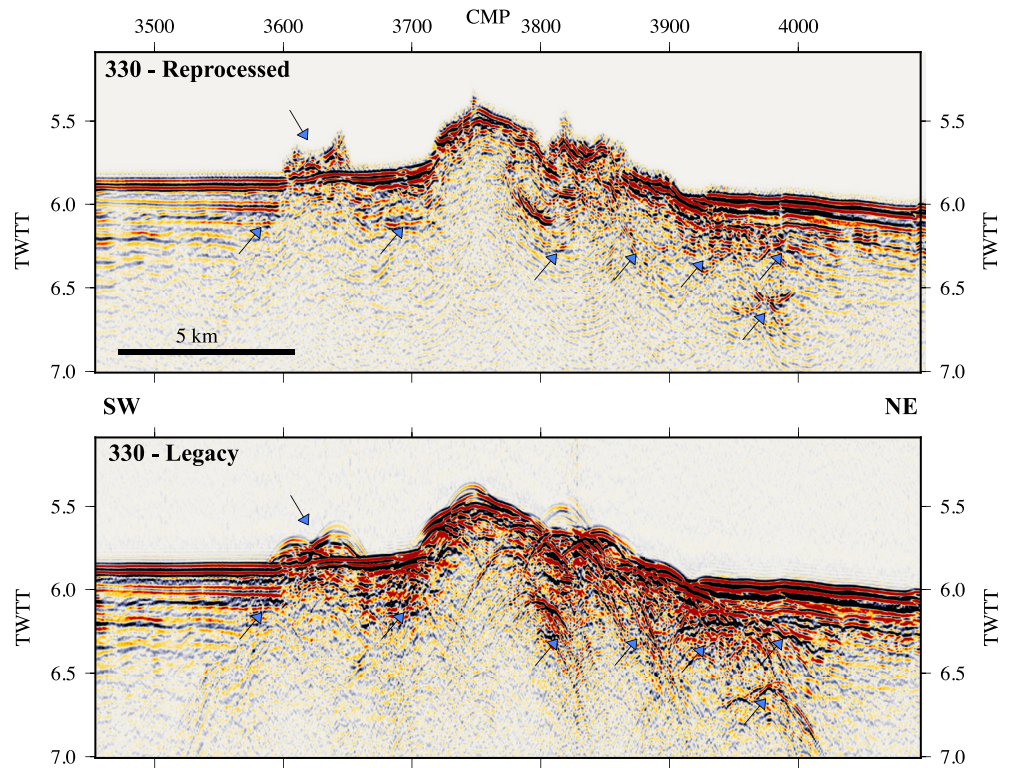


**Figure 10.** Post-stack reprocessed (top) and legacy (bottom) seismic images of Line 330 in the vicinity of two small seamounts in the flexural moat south of Oahu. Improvements from post-stack reprocessing include reduced ringing and very low frequencies, better-imaged sediment and bathymetry, and a clearer oceanic crust reflector. Segments of oceanic crust (blue arrows) and a possible deeper feature (CMP 3980, TWTT 6.6 s) are now interpretable between volcanic features after post-stack processing of the legacy data. An out-of-plane seamount is also more clearly imaged at CMP 3630 in the reprocessed data, while imaging is improved on steeply dipping features as well.

this, the best fit parameter pair that minimizes the Root Mean Square (RMS) difference between the observed picks and the calculated depth to the top of oceanic crust is determined. These parameters were used as a central point about which a Monte Carlo optimization scheme using the fast bounded simulated annealing algorithm was employed to find the true best fitting parameters. Specifically, 1,000 optimizations were run with uniform random starting points about the grid search solution, and all bounded simulated annealing solutions were then used as inputs into respective gradient descent routines to ensure a minimum had been found for every optimization. The

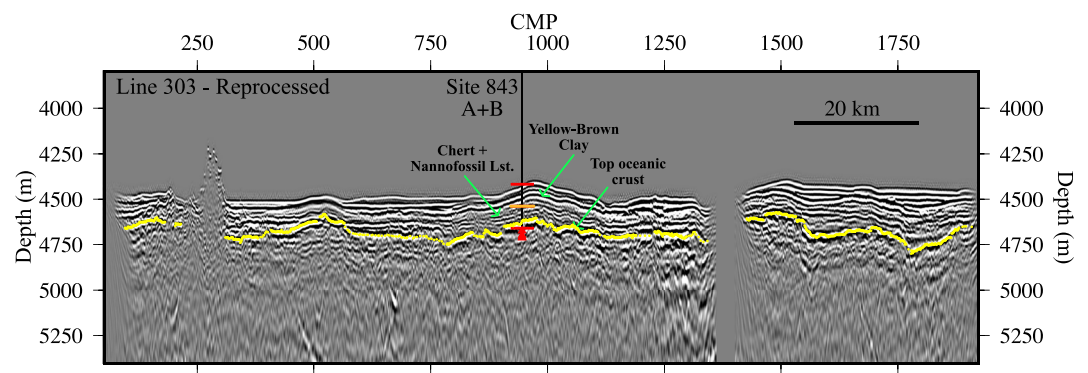


**Figure 11.** Interpretation of top of oceanic crust (yellow) along reprocessed Line 303 (see Figure 7). Ocean Drilling Project drill sites 843A and 843B (Shipboard Scientific Party, 1992) sampled Yellow-Brown clay, Chert and Nannofossil Limestone and top of oceanic basement. Short orange line shows depth to the top of the Chert and Nannofossil Limestone. Yellow filled circles show the top of the oceanic basement as picked on the seismic data.

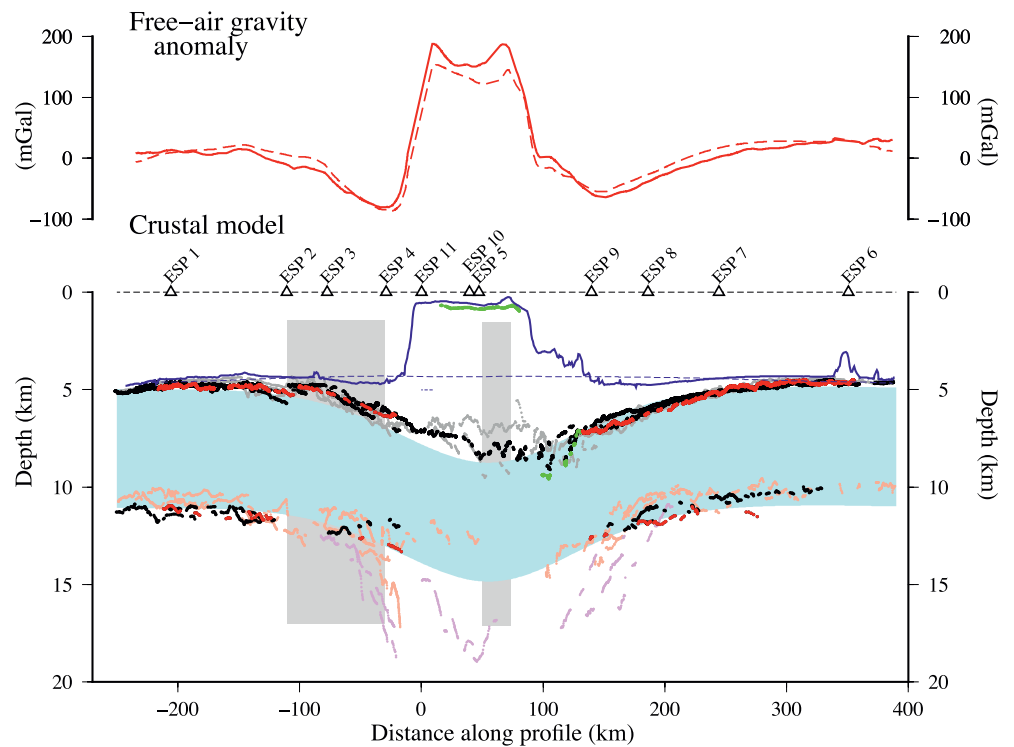


**Figure 12.** Comparison of the legacy and reprocessed reflector picks to the predicted top and base of oceanic crust based on a simple model of crustal structure and flexure. Red filled points show top and base of oceanic crust from the reprocessed two-ship data acquired along Lines 301 and 314. Black filled points show the same reflectors from the reprocessed single ship data acquired along Lines 330–332. Green filled points show reflectors from reprocessed data along Constant Offset Profile (COP) 5 and COP E (Line 313, Figure 1) which are interpreted as picks from within the edifice and its base, respectively. Light colored filled circles show the legacy picks associated with “Reflectors 2, 3, and 4” (see Watts and ten Brink (1989)). Blue dashed line shows the Hawaiian swell crest obtained by median filtering ( $w = 500$  km) the bathymetry grid. The light blue shaded region and the dashed red line show the predicted crustal structure and gravity anomaly based on a simple model of flexure with surface (bathymetric) loading, elastic thickness,  $T_e$ , of 20.9 km and densities for the load, average infill, crust and mantle of 2,737, 2,418, 2,800, and 3,330  $\text{kg m}^{-3}$ , respectively. Gray filled boxes show where the multistranded Molokai Fracture Zone intersects the profile according to Matthews et al. (2011).

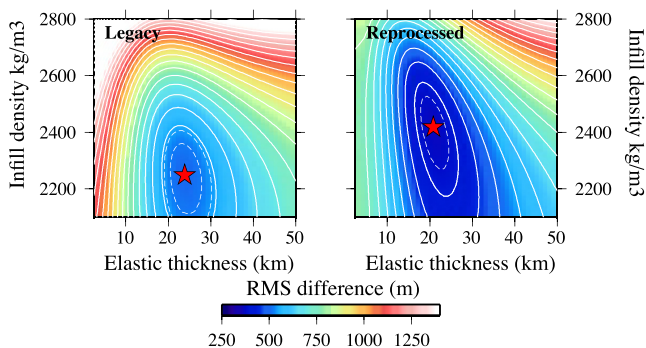


**Figure 13.** Comparison of the Root Mean Square of the difference between observed and calculated depth to the top of oceanic crust. Observed depths are based on picks of the top of oceanic crust from the RC2308 legacy data and reprocessed data along Lines 301, 314, and 329–332. The calculated depths are based on a simple model of flexure with a surface (bathymetric) load defined by a  $1 \times 1$  min GEBCO 2020 bathymetry grid, an assumed load density of 2,737  $\text{kg m}^{-3}$ , uniform values of  $T_e$  in the range 0–50 km and average densities of infill in the range 2,100–2,800  $\text{kg m}^{-3}$ . The red filled stars show the optimal misfit minima (Table 1).

RMS plots produced by the initial grid-search routine (Figure 13) show well defined minima and that reprocessing of the legacy data set has resulted in a significantly lower (by ~38%) RMS (Table 1, Rows 1 and 2).

The crustal structure corresponding to the  $T_e$  (20.9 km) and average infill density (2,418  $\text{kg m}^{-3}$ ) that best fits the reprocessed seismic data picks of the top of oceanic crust (RMS = 364.2 m) is illustrated along the line of projection in Figure 12 by the blue shaded region. Despite the good visual fit of the solution there are discrepancies. Most notable are in the region of the MFZ and beneath the edifice where the calculated depth to top of the oceanic crust is some 0.5–0.7 km deeper than the observed. There are also less obvious discrepancies in flanking moat regions where the wavelength of the calculated flexure appears too short compared to the observed.

The discrepancies in the seismic data are also manifest in the amplitude and wavelength of the free-air gravity anomaly. The RMS difference between observed and calculated gravity anomaly is 14.5 mGal. The calculated “high” anomaly over the edifice generally underpredicts the amplitude of the observed free-air gravity anomaly while the calculated “low” anomaly over the flanking moats is generally too short in wavelength compared to the observed. Both observations are suggestive of a higher elastic thickness

**Table 1**  
*The Root Mean Square Difference Between Observed Legacy and Reprocessed Data Sets and the Calculated Depths to the Top of Oceanic Crust Based on a 3-Dimensional Simple Elastic Plate (Flexure) Model*

Data sets	Number of digitized picks	Elastic thickness, $T_e$ (km)	Average infill density ( $\text{kg m}^{-3}$ )	Top oceanic crust RMS (m)
RC2308 Legacy	4,960	23.8	2,249	511.2
<b>RC2308 Reprocessed</b>	<b>22,369</b>	<b>20.9</b>	<b>2,418</b>	<b>364.2</b>

Note. Data in bold font are plotted in Figure 12.

and, possibly, a higher average infill density; we explore the impact of other factors on the estimated elastic thickness in the discussion.

## 6. Discussion

The flexure modeling and the reprocessing of legacy seismic data undertaken in this study provides the opportunity to obtain new insights into rheological properties of ~82.5–97.5 Ma Pacific oceanic lithosphere and to evaluate the scientific potential for undertaking such reprocessing on other similar legacy data sets.

### 6.1. Comparison With Previous $T_e$ Values

There have been a number of previous studies that have estimated the elastic thickness of the lithosphere,  $T_e$ , in the vicinity of the Hawaiian Islands (e.g., Gunn, 1943; Kunze, 1980; McNutt & Shure, 1986; Suyenaga, 1979; Walcott, 1970; Watts, 1978, 1979; Watts & Cochran, 1974; Watts & ten Brink, 1989; Wessel, 1993; Zhong & Watts, 2013). Of relevance to this study are the estimates of Watts and ten Brink (1989), Wessel (1993), and Zhong and Watts (2013), each of which were based on the RC2308 legacy seismic data set.

Watts and ten Brink (1989) suggested the best fit to the top of oceanic crust reflector in the legacy data set was for  $T_e = 40$  km and an average infill density of  $2,300 \text{ kg m}^{-3}$ , assuming a load density of  $2,800 \text{ kg m}^{-3}$ , a Young's modulus of 100 GPa and a Poisson's ratio of 0.25. The RMS difference between the observed depth to the top of the oceanic crust and the calculated depth based on these parameters was 540 m. The study was based, however, on a grid of  $5 \times 5$  min averages of shipboard single beam echosounder data offshore and a ETOPO5 contour-derived data set onshore. Another problem was that the load was separated assuming a uniform base of 4.5 km below sea level and so bathymetric features such as the Hawaiian swell crest, landslide material and outlying seamounts were included in the load and this together with its relatively high density assumed for the load suggest the load and hence the  $T_e$  may well have been overestimated.

In this study, we have used a load based on a  $1 \times 1$  min GEBCO + SRTM 2020 grid which incorporates a significant component of multibeam (swath) bathymetry data in addition to the single beam data and so is of a significantly higher resolution than the one used in Watts and ten Brink (1989). Furthermore, the load was extracted using a base given by the mean topography (5.019 km) and by masking out any flexural effects associated with landslide material and outlying seamounts which may have formed in a different tectonic setting in relation to the East Pacific Rise than the Hawaiian Ridge. The load density was also not assumed but derived instead from a preliminary analysis of seismic refraction data acquired along Line 2 (Dunn et al., 2019) to be  $2,737 \text{ kg m}^{-3}$ . The resulting  $T_e$  of 23.8 and 20.9 km for the legacy and reprocessed data sets respectively (Table 1, Rows 1 and 2) is significantly smaller than that derived by Watts and ten Brink (1989).

A final difficulty with the Watts and ten Brink (1989) study, pointed out by Wessel (1993), was that it did not correct the depth to the top and base of oceanic crust for the effects of the Hawaiian swell, a mid-plate bathymetric rise that has been attributed to an upwelling in the mantle associated with the Hawaiian plume (Watts, 1976; Zhong & Watts, 2002), not to plate flexure. Wessel (1993) used a best fitting “super-Gaussian” to remove the swell from the legacy seismic data set and found  $T_e = 25$  km which was significantly lower than that deduced by Watts and ten Brink (1989) and an average infill density of  $2,550 \text{ kg m}^{-3}$  which was significantly higher. He also suggested spatial changes in elastic thickness with higher  $T_e$  north of the northern offset of the MFZ (~30 km) and lower  $T_e$  to the south (~20 km).

Although a relatively small effect because our line of projection mainly follows the crest of the swell, we followed Wessel (1993) and corrected both the legacy and reprocessed picks. We found that a simple median filter ( $w = 500$  km) satisfactorily isolated the Hawaiian swell since tests showed that such a filter accounts well for both the flank and crest of the swell in the absence of the Hawaiian Island volcanic loads and their associated flexure (see thin dashed blue line in Figure 12). The RMS plots for the swell corrected legacy and reprocessed seismic data produced by the initial grid-search routine show well-defined minima (Figure 14). The best fit of  $T_e = 28.2$  km and average infill density of  $2,547 \text{ kg m}^{-3}$  (Table 2, Row 1) are in close agreement with the

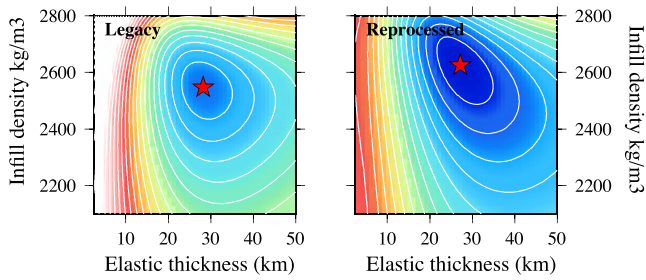


**Figure 14.** Comparison of the Root Mean Square of the difference between observed and calculated depth to the top of oceanic crust. Observed depths are based on the same picks as in Figure 12 but have been corrected for the effects of the Hawaiian mid-plate swell. The calculated depths are based on the same flexure model, load densities, and ranges of infill density and  $T_e$  as in Figure 12. The red filled stars show the optimal misfit minima (Rows 1–2, Table 2).

values deduced by Wessel (1993) from the same data set, but a different load geometry and density. The swell corrected reprocessed data set (Table 2, Row 2) suggests a slightly lower  $T_e$  (27.2 km) and higher average infill density ( $2,625 \text{ kg m}^{-3}$ ) than the swell corrected legacy data set.

We note that the RMS for the swell corrected reprocessed data (412.1 m, Table 2, Row 2) is not as low as might be expected; it is similar to the uncorrected data (364.2 m, Table 1, Row 2). We attribute this to the main misfit in the data, which is associated with the region of the MFZ, southwest of Oahu. The shallower top of oceanic crust in the MFZ is apparently better accounted for in the reprocessed data by the low elastic thickness deduced from the uncorrected data than the high elastic thickness deduced from the swell corrected data.

The top of oceanic crust systematically shallows in the MFZ by  $\sim 0.6 \text{ km}$  which suggests that it is unrelated to mechanical loading by the Hawaiian Islands since such loading would induce more, not less, flexure than is observed. We are uncertain of the origin of the shallowing. Recent age grids (Seton et al., 2020)

suggest the seafloor in the vicinity of the MFZ is  $\sim 94 \text{ Ma}$  which should be  $5,684 \text{ m}$  deep in the absence of a mid-plate swell according to the cooling plate model. A shallowing of  $0.6 \text{ km}$  in the MFZ could therefore be indicative of younger seafloor. However, this would require a seafloor age of  $\sim 54 \text{ Ma}$  which seems unlikely. A more likely explanation is crustal thickening due to magmatic addition. Irrespective, the shallower seafloor would be expected to have been in some form of isostatic equilibrium prior to flexure. For example, the observed shallowing of  $0.6 \text{ km}$  could be explained either by a Pratt-Hayford model of isostasy with a compensation depth of  $125 \text{ km}$  and an average sub-crustal mantle density  $11.6 \text{ kg m}^{-3}$  less than expected for  $94 \text{ Ma}$  oceanic lithosphere or by an Airy-Heiskanen model of isostasy with a compensation depth at zero elevation of  $31.2 \text{ km}$  and crust that is  $2.6 \text{ km}$  thicker than expected.

Figure 15 compares the reprocessed swell corrected picks that include an isostatic correction in the vicinity of the MFZ to the predictions of the top and base of oceanic crust based on a simple model of flexure. The optimal fit is for  $T_e = 26.7 \text{ km}$  and an average infill density of  $2,701 \text{ kg m}^{-3}$  (Table 2, Row 3). The RMS difference between observed and calculated depths is  $305.5 \text{ m}$ , which is  $\sim 26\%$  lower than that without the isostatic correction. The RMS was reduced even further ( $299.7 \text{ m}$ ) when account was taken of possible bias due to the different number of picks in the edifice, moat, and bulge regions. The fit to the observed seismic data along the line of projection is excellent ( $\text{RMS} = 338.4 \text{ m}$ ), as is the fit to the observed free-air gravity anomaly ( $\text{RMS} = 7.0 \text{ mGal}$ ) based on the  $1 \times 1 \text{ min}$  satellite-derived grid (V29.1) of Sandwell et al. (2019). We therefore consider the latter parameter pair as the optimum fit to the reprocessed *Conrad* seismic data.

## 6.2. Variable Load and Infill Densities

We have so far assumed a fixed load density ( $2,737 \text{ kg m}^{-3}$ ) in the flexure calculations. As Minshull and Charvis (2001) and others have shown, load densities can impact the  $T_e$  estimate. Table S1 and Figure S5 in Supporting Information S1 show the effect of different assumed load densities. Increasing the load density, for example, results in a higher  $T_e$  (by  $1 \text{ km}$ ) and a lower infill density (by  $40 \text{ kg m}^{-3}$ ). The reason for this is that

**Table 2**

*The Root Mean Square Difference Between Observed Legacy and Reprocessed Data Sets and the Calculated Depths to the Top of Oceanic Crust Based on a 3-Dimensional Elastic Plate (Flexure) Models*

Data sets	Number of digitized picks	Elastic thickness, $T_e$ (km)	Average infill density ( $\text{kg m}^{-3}$ )	Top oceanic crust RMS (m)
RC2308 Legacy Swell corrected	4,960	28.2	2,547	503.1
RC2308 Reprocessed Swell corrected	22,369	27.2	2,625	412.1
<b>RC2308 Reprocessed Swell + Isostatic corrected</b>	<b>22,369</b>	<b>26.7</b>	<b>2,701</b>	<b>305.5</b>

*Note.* The observed data have been corrected for the effects of the Hawaiian mid-plate swell and the MFZ. Data in bold font are plotted in Figure 15

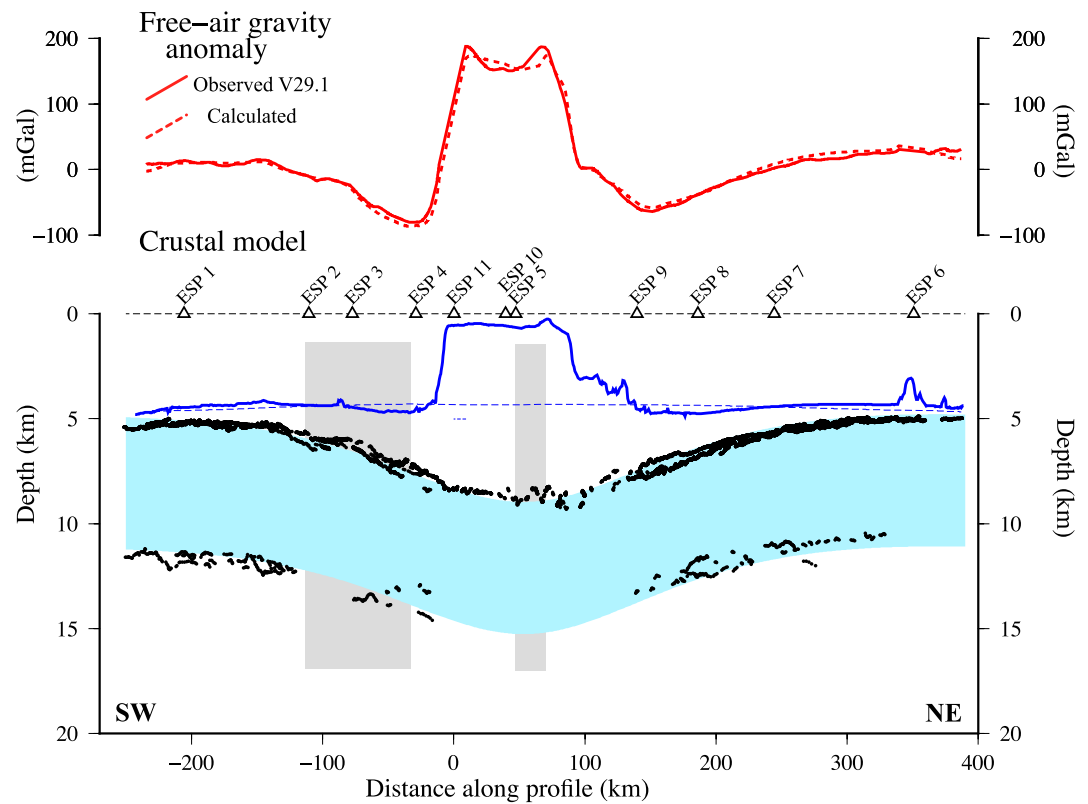


**Figure 15.** Comparison of the swell corrected and isostatically corrected reprocessed reflector picks to the predicted top and base of oceanic crust based on a simple model of flexure. Black filled points show picks along both the single ship and two-ship data. Dark blue dashed line shows the Hawaiian swell crest obtained by median filtering ( $w = 500$  km) of the bathymetry grid. The light blue shaded region and the dashed red line show the predicted crustal structure and gravity anomaly based on a simple model of flexure with surface (bathymetric) loading, elastic thickness,  $T_e$ , of 26.7 km and densities for the load, average infill, crust and mantle of 2,737, 2,701, 2,800, and 3,330  $\text{kg m}^{-3}$ , respectively. The Molokai Fracture Zone, shown in shaded gray, is defined in Figure 12.

increasing the load density results in a larger flexure and so requires a higher  $T_e$  and smaller infill density to produce the same depth to the top of oceanic crust. Decreasing the load density has the opposite effect and requires a lower  $T_e$  (by 1 km) and higher infill density (by 50  $\text{kg m}^{-3}$ ). The RMS difference in each case is, as expected, similar.

We also assumed that the infill density and hence the restoring force that acts on the flexed plate is uniform and does not vary laterally from the bulges through the moats to beneath the edifice. However, it is likely that the infill density will vary either side and beneath the Hawaiian Islands. The bulge, for example, is an upward flexure that displaces water while the region beneath the edifice is a downward flexure which is likely to comprise material with a similar density to that of the load. The intermediate infill in the flanking moats is likely to mainly comprise material derived from the edifice by mass wasting from the islands and hence, depending on the amount of volcanoclastic material which may also infill the moats, to be lower density than that of the edifice.

To investigate variations in infill density we compared the reprocessed swell corrected data to the calculated flexure based on the 3-dimensional finite difference code of Cardozo and Jordan (2001). We assumed the infill density beneath the load was the same as that of the load and that the infill density in bulge regions (defined as a positive flexure) was water. We then repeated the grid-search routine using the reprocessed swell corrected seismic data, but this time searched for the best fit of  $T_e$  and the infill density in just the moat regions. The RMS minimum (413.2 m) corresponds to a best fit  $T_e$  and moat infill density estimate of 24.3 km and 2,550  $\text{kg m}^{-3}$  respectively (Figure 16). The infill beneath the edifice was 2,737  $\text{kg m}^{-3}$  and so the average infill in this case would be 2,643  $\text{kg m}^{-3}$  which is similar to (but not the same as) the value we determined previously using the same data set for the average infill density (2,625  $\text{kg m}^{-3}$ ). Therefore, the average infill density deduced in our

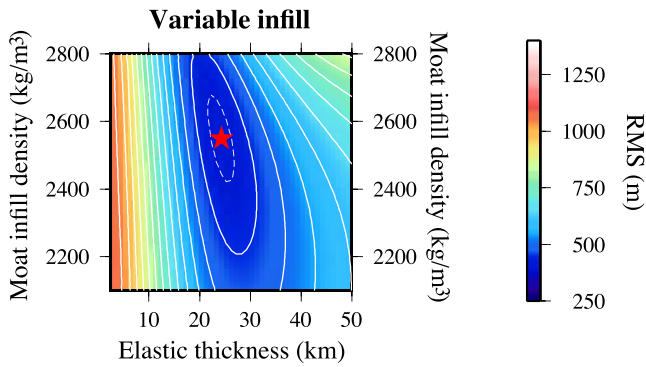


**Figure 16.** Comparison of the Root Mean Square (RMS) of the difference between observed and calculated depth to the top of oceanic crust using a variable moat infill density model. Observed depths are based on picks of the top of oceanic crust from the RC2308 reprocessed swell corrected data. The calculated depths are based on a finite difference model (Cardozo & Jordan, 2001) with a surface (bathymetric) load defined by a  $1 \times 1$  min swath grid, assumed load density of  $2,737 \text{ kg m}^{-3}$ , uniform values of  $T_e$  in the range 0–50 km and moat infill densities (vertical axis) in the range  $2,100\text{--}2,800 \text{ kg m}^{-3}$ . The RMS minimum (413.2 m) corresponds to a best fit estimate of 24.3 km and  $2,550 \text{ kg m}^{-3}$  for the elastic thickness and the moat infill density, respectively. The infill density inverted for using the swell corrected picks (Table 2, Row 2) of  $2,625 \text{ kg m}^{-3}$  therefore appears to be approximately an average of the moat infill ( $2,550 \text{ kg m}^{-3}$ ) and the infill assumed immediately beneath the edifice ( $2,737 \text{ kg m}^{-3}$ ).

optimal searches can be considered approximately as an arithmetic average of the infill density beneath the edifice and the infill density in the moats.

### 6.3. Comparison With Langseth Line 2

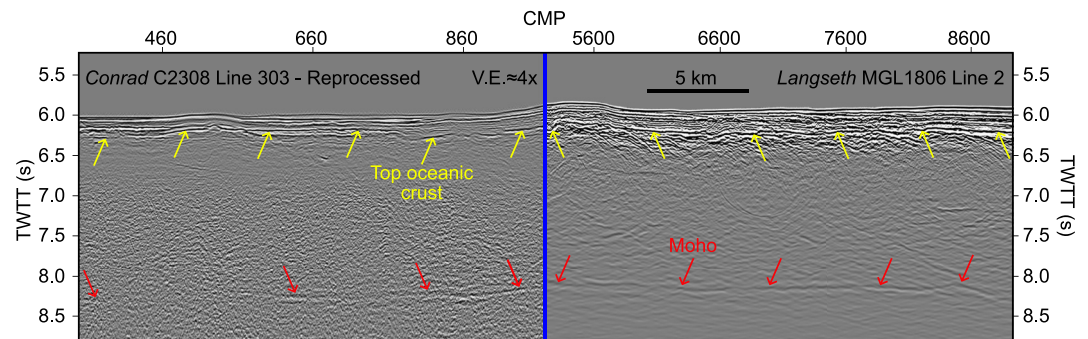
The *Conrad* MCS data were acquired with a relatively small air gun array and short streamer compared to that used during the *Langseth* cruise. It is instructive therefore to compare the two data sets.

Figure 17 compares the *Conrad* reprocessed Line 303 and *Langseth* Line 2 data at the point of their intersection on the flexural bulge southwest of Oahu. The Moho is well defined in both MCS data sets where it appears to be represented by a single impulsive event. The profiles were acquired with two single ships, with one (*Langseth*) having a significantly larger volume airgun array and longer streamer than the other (*Conrad*) yet the visual character and frequency content of the Moho is strikingly similar in both data sets. We suspect this is due to the similar angle mutes used when imaging the Moho using both data sets, combined with similar depth-dependent bandpass filtering and the intrinsic frequency-dependent attenuation of the Earth. That is to say, the higher frequency components of the *Langseth's* airgun array are likely attenuated while traveling to the depth of the Moho and back to receivers, resulting in an image of the Moho comparable in quality to that produced by *Conrad*. The top of oceanic crust and the overlying sedimentary structure, on the other hand, appears to be less well resolved in the *Conrad* data than in the *Langseth* data. We attribute this to the ringing in the *Conrad* data due to a residual bubble pulse and/or an untuned airgun array and to the higher frequency components of *Langseth's* tuned array.

The similarities and differences between the *Conrad* and *Langseth* MCS data sets are well seen in Figure S6 in Supporting Information S1 which shows a normalized amplitude spectrum of a window of the data close to the point of intersection.

### 6.4. Implications for Other Conrad Data Sets

The reprocessing of the legacy data outlined in this paper and its successful application to a hotspot generated seamount chain in a plate interior has been based only the seismic data acquired during a single cruise RC2308 of *Conrad* in 1982. R/V *Robert D. Conrad* was involved, however, in many other seismic experiments in each of the world's oceans and their margins (Figure 18). Notable examples were the surveys carried out by; Diebold et al. (1981) of the Venezuela basin—Cruises RC1904 and RC2103; Herron et al. (1978) and Detrick et al. (1987) of the East Pacific Rise at  $9^\circ$  and  $13^\circ\text{N}$ —Cruises RC2002 and RC2607; Ludwig and Rabinowitz (1982) of



**Figure 17.** Comparison of a time section of *Conrad* RC2308 Line 303 and *Langseth* MGL1806 Line 2 at the point of their intersection (Blue solid line) on the flexural bulge southwest of Oahu (Figure 1). Left-hand panel = *Conrad*. Right-panel = *Langseth*.



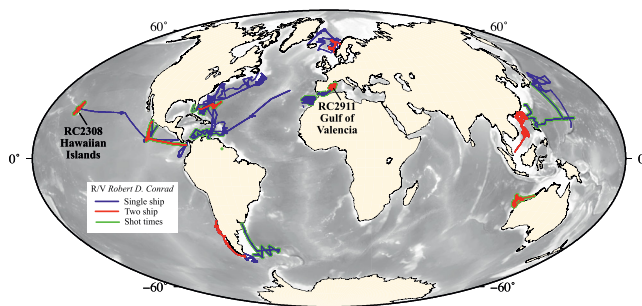


**Figure 18.** World map showing all the *Robert D. Conrad* single-ship and two-ship seismic cruises. Red = two-ship experiments. Blue = single ship experiments. Green = cruises with shot times that can be downloaded from the MGDS website. Cruises RC2308 and RC2911 were the first and last two-ship experiments that involved *Conrad*. Note that most seismic experiments of *Conrad* were focussed on the passive and active continental margins.

the Falklands/Malvinas Plateau and Trough—Cruise RC2106; Talwani et al. (1981) of the Norwegian Sea and Voring Plateau—Cruises RC2113 and RC2114; Holik and Rabinowitz (1991) of the Morocco passive margin—Cruises RC2405 and RC2406; Nissen et al. (1995) of the South China Sea passive margin—Cruises RC2612 - RC2614; White et al. (1990) of the Blake Spur Fracture Zone—Cruise RC2810, western Atlantic; Bangs and Cande (1997) of the Chile active margin—RC2901 and RC2902; and Watts et al. (1990) of the Gulf of Valencia and Alboran Sea, Western Mediterranean—RC2911.

The wide range of geological features sampled—from mid-ocean ridges through oceanic plateaus to passive and active margins—suggest therefore that the seismic data from these cruises should be similarly reprocessed using modern processing algorithms such as those used here. We illustrate the benefits in Supporting Information S1 where we compare, in detail, segments of the legacy and reprocessed MCS data acquired during *Conrad* cruise RC2911 along Line 819 in the Gulf of Valencia (Watts et al., 1990) and MCS Line 827 in the Alboran Sea (Watts et al., 1993). Reprocessing (e.g.,

Figures S9–S14 in Supporting Information S1) reveals new geological features not previously recognized in the RC2911 seismic data or reproduced in subsequent publications. These features include a set of steep faults which offset Plio-Pleistocene prograding deltaic sediments in the northern Gulf of Valencia, the internal structure of a stratigraphic unit bounded by unconformities that comprise the Messinian Erosional Surface in the southern Alboran Sea, and a lower continental crust that is characterized by “lamellae” rather than “crocodiles” and is underlain by a bright continuous Moho.

## 7. Conclusions

- Modern methods of processing of seismic data acquired during the 1982 single ship and two-ship *Conrad* RC2308 cruise to the Hawaiian Islands have significantly enhanced the value of this legacy data set, especially through the application of improved denoise, deconvolution, and migration technologies.
- Picks of reflectors on depth converted reprocessed data at the top of oceanic crust, within and at the base of the volcanic edifice, and Moho show them to be significantly smoother than the picks derived from the legacy data, for example, those used in Watts and ten Brink (1989) and subsequent rheological studies.
- The smoother picks result in a 38% reduction in the RMS difference between the observed reflector depths and the calculated depths based on analytical models of plate flexure and, hence, have yielded more reliable parameters for robust estimate of the elastic thickness and average infill density.
- A 2-parameter inversion of a swell-corrected reprocessed pick data set reveals a best fit elastic thickness,  $T_e$ , for the Hawaiian Ridge in the region of the islands of Oahu and Molokai of 26.7 km and an average infill density of  $2,701 \text{ kg m}^{-3}$ . This parameter pair yields an RMS fit between the observed and calculated depth to top of oceanic crust and the observed and calculated free-air gravity anomaly of 305.5 m and 7.0 mGal respectively.
- Tests show our results to depend weakly on the load density assumed and that our estimates of the average infill density are, in fact, close to what would be predicted from an arithmetic average of the moat infill density and the density of the infill that underlies a volcanic edifice.
- The seismic reflection profile data acquired by the Lamont-Doherty Geological Observatory operated research vessel *R/V Robert D. Conrad* during 1975–1988 is an important legacy data set that may be used to re-examine not only the thermal and mechanical properties of oceanic lithosphere but also the structure, stratigraphy and evolution of the world's ocean basins and their margins.

## Data Availability Statement

The reprocessed *Conrad* SEG-Y data used in this research (Cilli et al., 2023) are available for download from the Marine Geoscience Data System (MGDS) at <https://www.marine-geo.org/tools/search/entry.php?id=RC2308> and in GeoMapApp ([geomapapp.org](http://geomapapp.org)). The data, which includes navigation in the SEG-Y headers, has been

assigned a DOI of <https://doi.org/10.26022/IEDA/331293>. The field data (Buhl & Watts, 1982) for RC2308 will become available at the same URL before 31 December 2023.

### Acknowledgments

This work was funded by a NERC Grant NE/S01036X/1 and NSF Grant OCE-2051501. We are grateful to ION Geophysical for reading the legacy 9-track seismic data tapes and for providing Lamont-Doherty Earth Observatory with access to the digital RC2308 legacy data prior to the *R/V Marcus G. Langseth* 2018 cruise and Joyce Alsop, Roseanne Weissel and Suzanne Carbotte for assistance accessing the data. We thank Shearwater Geoservices Ltd for provision of academic licenses to run the *Reveal* seismic data processing software to Oxford and to Emerson for provision of academic licenses to Lamont-Doherty Earth Observatory to the *Paradigm* processing and interpretation software suite. Figures were constructed using *Reveal* and GMT (Wessel & Luis, 2017) software.

### References

- Bangs, N. L., & Cande, S. (1997). Episodic development of a convergent margin inferred from structures and processes along the southern Chile margin. *Tectonics*, *16*(3), 489–503. <https://doi.org/10.1029/97tc00494>
- Boston, B., Shillington, D. J., Dunn, R., Watts, A. B., Grevenmeyer, I., Gómez de la Peña, L., et al. (2019). The crustal and upper mantle structure of the Hawaiian-Emperor Seamount Chain from marine seismic data. In *Abstract T41B-06 talk presented at the 2019 fall meeting*. AGU.
- Brocher, T. M., & ten Brink, U. S. (1987). Variations in Oceanic Layer 2 elastic velocities near Hawaii and their correlation to lithospheric flexure. *Journal of Geophysical Research*, *92*(B3), 2647–2661. <https://doi.org/10.1029/jb092ib03p02647>
- Buhl, P., & Watts, A. B. (1982). RC2308 Field data: Bathymetry, gravity, magnetic and seismic reflection and refraction [Dataset]. Retrieved from <https://www.marine-geo.org/tools/search/entry.php?id=RC2308#datasets>
- Cardozo, N., & Jordan, T. (2001). Causes of spatially variable tectonic subsidence in the Miocene Bermejo foreland basin, Argentina. *Basin Research*, *13*(3), 335–357. <https://doi.org/10.1046/j.0950-091x.2001.00154.x>
- Cilli, P., Watts, A. B., Boston, B., & Shillington, D. J. (2023). RC2308 Reprocessed seismic reflection data [Dataset]. <https://doi.org/10.26022/IEDA/331293>
- Detrick, R. S., Buhl, P., Vera, E. E., Mutter, J. C., Orcutt, J. A., Madsen, J. A., & Brocher, T. M. (1987). Multichannel seismic imaging of the axial magma chamber along the East Pacific Rise between 9°N and 13°N. *Nature*, *326*(6108), 35–41. <https://doi.org/10.1038/326035a0>
- Diebold, J. B., Stoffa, P. L., Buhl, P., & Truchan, M. (1981). Venezuela basin crustal structure. *Journal of Geophysical Research*, *86*(B9), 7901–7923. <https://doi.org/10.1029/jb086ib09p07901>
- Dunn, R., Shillington, D. J., Watts, A. B., Boston, B., Gómez de la Peña, L., Grevenmeyer, I., et al. (2019). Lithospheric structure across the Hawaiian-Emperor Seamount Chain from seismic wide angle reflection-refraction tomography. In *Abstract T43F-0515 presented at the 2019 fall meeting*. AGU.
- Gunn, R. (1943). A quantitative study of isobaric equilibrium and gravity anomalies in the Hawaiian Islands. *Journal of the Franklin Institute*, *236*(4), 373–390. [https://doi.org/10.1016/s0016-0032\(43\)90275-3](https://doi.org/10.1016/s0016-0032(43)90275-3)
- Herron, T. J., Ludwig, W. J., Stoff, P. L., Kan, T. K., & Buhl, P. (1978). Structure of the East Pacific Rise crest from multichannel seismic reflection data. *Journal of Geophysical Research*, *83*(B2), 798–804. <https://doi.org/10.1029/jb083ib02p00798>
- Holik, J. S., Rabinowitz, P. D., & Austin, J. A. (1991). Effects of Canary hotspot volcanism on structure of oceanic crust off Morocco. *Journal of Geophysical Research*, *96*(B7), 12039–12067. <https://doi.org/10.1029/91jb00709>
- Kunze, A. W. G. (1980). On the flexural rigidity and effective viscosity of the lithosphere in the Hawaiian area. *Tectonophysics*, *69*(3–4), T1–T8. [https://doi.org/10.1016/0040-1951\(80\)90208-5](https://doi.org/10.1016/0040-1951(80)90208-5)
- Leahy, G. M., Collins, J. A., Wolfe, C. J., Laske, G., & Solomon, S. C. (2010). Underplating of the Hawaiian Swell: Evidence from teleseismic receiver functions. *Geophysical Journal International*, *183*(1), 313–329. <https://doi.org/10.1111/j.1365-246x.2010.04720.x>
- Leahy, G. M., & Park, J. (2005). Hunting for oceanic island Moho. *Geophysical Journal International*, *160*(3), 1020–1026. <https://doi.org/10.1111/j.1365-1246x.2005.02562.x>
- Lewis, S. D., & Hayes, D. E. (1989). Plate convergence and deformation, north Luzon Ridge, Philippines. *Tectonophysics*, *168*(1–3), 221–237. [https://doi.org/10.1016/0040-1951\(89\)90377-6](https://doi.org/10.1016/0040-1951(89)90377-6)
- Lindwall, D. A. (1988a). *Deep crustal structure under and near the Hawaiian Islands*, (p. 122). Ph. D. thesis, University of Hawaii.
- Lindwall, D. A. (1988b). A two-dimensional seismic investigation of crustal structure under the Hawaiian Islands near Oahu and Kauai. *Journal of Geophysical Research*, *93*(B10), 12107–12122. <https://doi.org/10.1029/jb093ib10p12107>
- Ludwig, W. J., & Rabinowitz, P. D. (1982). The collision complex of the North Scotia ridge. *Journal of Geophysical Research*, *87*(B5), 3731–3740. <https://doi.org/10.1029/jb087ib05p03731>
- Matthews, K. J., Müller, R. D., Wessel, P., & Whittaker, J. M. (2011). The tectonic fabric of the ocean basins. *Journal of Geophysical Research*, *116*(B12), B12109. <https://doi.org/10.1029/2011JB008413>
- McNutt, M. K., & Shure, L. (1986). Estimating the compensation depth of the Hawaiian Swell with linear filters. *Journal of Geophysical Research*, *91*(B14), 13915–13923. <https://doi.org/10.1029/jb091ib14p13915>
- Minshull, T. A., & Charvis, P. (2001). Ocean island densities and models of lithospheric flexure. *Geophysical Journal International*, *145*(3), 731–739. <https://doi.org/10.1046/j.0956-540x.2001.01422.x>
- Minshull, T. A., White, R. S., Mutter, J. C., Buhl, P., Detrick, R. S., Williams, C. A., & Morris, E. (1991). Crustal structure at the Blake Spur fracture zone from expanding spread profiles. *Journal of Geophysical Research*, *96*(B6), 9955–9984. <https://doi.org/10.1029/91JB00431>
- Morgan, J. K., Moore, G. F., & Clague, D. A. (2003). Slope failure and volcanic spreading along the submarine south flank of Kilauea volcano, Hawaii. *Journal of Geophysical Research*, *108*(B9), 2415. <https://doi.org/10.1029/2003JB002411>
- Mutter, J. C., Talwani, M., & Stoffa, P. L. (1984). Evidence for a thick oceanic crust adjacent to the Norwegian margin. *Journal of Geophysical Research*, *89*(B1), 483–502. <https://doi.org/10.1029/jb089ib01p00483>
- Nissen, S. S., Hayes, D. E., Buhl, P., Diebold, J., Yao, B., Zeng, W., & Chen, Y. (1995). Deep penetration seismic soundings across the northern margin of the South China Sea. *Journal of Geophysical Research*, *100*(B11), 22407–22433. <https://doi.org/10.1029/95jb01866>
- Sandwell, D. T., Harper, H., Tozer, B., & Smith, W. H. F. (2019). Gravity field recovery from geodetic altimeter missions. *Advances in Space Research*, *68*(2), 1059–1072. <https://doi.org/10.1016/j.asr.2019.09.011>
- Seton, M., Müller, R. D., Zahirovic, S., Williams, S., Wright, N., Cannon, J., et al. (2020). A global dataset of present-day oceanic crustal age and seafloor spreading parameters. *Geochemistry, Geophysics, Geosystems*, *21*(10), e2020GC009214. <https://doi.org/10.1029/2020GC009214>
- Sheridan, R. E., Pastouret, L., & Mosditchian, G. (1978). Seismic stratigraphy and related lithofacies of the Blake-Bahama basin. In W. E. Benson & R. E. Sheridan (Eds.), *Initial reports of the deep sea drilling project*. U.S. Government Printing Office.
- Shipboard Scientific Party. (1992). Site 843. Initial Reports. In *Proceedings of the ocean drilling program* (Vol. 136, pp. 65–99).
- Suyenaga, W. (1979). Isostasy and flexure of the lithosphere under the Hawaiian Islands. *Journal of Geophysical Research*, *84*(B10), 5599–5604. <https://doi.org/10.1029/jb084ib10p05599>
- Talwani, M., Mutter, J., & Eldholm, O. (1981). The initiation of opening of the Norwegian Sea. *Oceanologica Acta*, 23–30.
- ten Brink, U. S. (1986). *Lithospheric flexure and Hawaiian volcanism: A multichannel seismic perspective*, (p. 219). Ph. D thesis, Columbia University.
- ten Brink, U. S., & Brocher, T. M. (1987). Multichannel seismic evidence for a subcrustal intrusive complex under Oahu and a model for Hawaiian volcanism. *Journal of Geophysical Research*, *92*(B13), 13687–13707. <https://doi.org/10.1029/jb092ib13p13687>

- Vera, E. E., & Diebold, J. B. (1994). Seismic imaging of oceanic layer 2A between 9°30'N and 10°N on the East Pacific Rise from two-ship wide-aperture profiles. *Journal of Geophysical Research*, 99(B2), 3031–3041. <https://doi.org/10.1029/93jb02107>
- Walcott, R. I. (1970). Flexure of the lithosphere at Hawaii. *Tectonophysics*, 9(5), 435–446. [https://doi.org/10.1016/0040-1951\(70\)90056-9](https://doi.org/10.1016/0040-1951(70)90056-9)
- Watts, A. B. (1976). Gravity and bathymetry in the central Pacific Ocean. *Journal of Geophysical Research*, 81(8), 1533–1553. <https://doi.org/10.1029/jb081i008p01533>
- Watts, A. B. (1978). An analysis of isostasy in the world's oceans: 1. Hawaiian-Emperor Seamount Chain. *Journal of Geophysical Research*, 83(B12), 5989–6004. <https://doi.org/10.1029/jb083ib12p05989>
- Watts, A. B. (1979). On geoid heights derived from GEOS 3 altimeter data along the Hawaiian-Emperor Seamount Chain. *Journal of Geophysical Research*, 84(B8), 3817–3826. <https://doi.org/10.1029/jb084ib08p03817>
- Watts, A. B., & Cochran, J. R. (1974). Gravity anomalies and flexure of the lithosphere along the Hawaiian-Emperor seamount chain. *Geophysical Journal of the Royal Astronomical Society*, 38(1), 119–141. <https://doi.org/10.1111/j.1365-246x.1974.tb04112.x>
- Watts, A. B., Platt, J., & Buhl, P. (1993). Tectonic evolution of the Alboran Sea basin. *Basin Research*, 5(3), 153–177. <https://doi.org/10.1111/j.1365-2117.1993.tb00063.x>
- Watts, A. B., ten Brink, U., Buhl, P., & Brocher, T. (1985). A multichannel seismic study of lithospheric flexure across the Hawaiian-Emperor seamount chain. *Nature*, 315(6015), 105–111. <https://doi.org/10.1038/315105a0>
- Watts, A. B., & ten Brink, U. S. (1989). Crustal structure, flexure and subsidence history of the Hawaiian Islands. *Journal of Geophysical Research*, 94(B8), 10473–10500. <https://doi.org/10.1029/jb094ib08p10473>
- Watts, A. B., Torné, M., Buhl, P., Mauffret, A., Pascal, G., & Pinet, B. (1990). Evidence for reflectors in the lower continental crust before rifting in the Valencia trough. *Nature*, 348(6302), 631–635. <https://doi.org/10.1038/348631a0>
- Wessel, P. (1993). A re-examination of the flexural deformation beneath the Hawaiian Islands. *Journal of Geophysical Research*, 98(B7), 12177–12190. <https://doi.org/10.1029/93jb00523>
- Wessel, P., & Luis, J. F. (2017). The GMT/MATLAB toolbox. *Geochemistry, Geophysics, Geosystems*, 18(2), 811–823. <https://doi.org/10.1002/2016GC006723>
- White, R. S., Detrick, R. S., Mutter, J. C., Buhl, P., Minshull, T. A., & Morris, E. (1990). New images of oceanic crustal structure. *Geology*, 18(5), 462–465. [https://doi.org/10.1130/0091-7613\(1990\)018<0462:nsiooc>2.3.co;2](https://doi.org/10.1130/0091-7613(1990)018<0462:nsiooc>2.3.co;2)
- Yilmaz, O. (2001). *Seismic data analysis* (p. 2027). Society Exploration Geophysicists Books.
- Zhong, S., & Watts, A. B. (2002). Constraints on the dynamics of mantle plumes from uplift of the Hawaiian Islands. *Earth and Planetary Science Letters*, 203(1), 105–116. [https://doi.org/10.1016/s0012-821x\(02\)00845-2](https://doi.org/10.1016/s0012-821x(02)00845-2)
- Zhong, S., & Watts, A. B. (2013). Lithospheric deformation induced by loading of the Hawaiian Islands and its implications for mantle rheology. *Journal of Geophysical Research: Solid Earth*, 118(11), 6025–6048. <https://doi.org/10.1002/2013JB010408>

## References From the Supporting Information

- Ayala, C., Torné, M., & Roca, E. (2015). A review of the current knowledge of the crustal and lithospheric structure of the Valencia trough Basin. *Boletín Geológico y Minero*, 126, 533–552.
- Collier, J., Buhl, P., Torné, M., & Watts, A. B. (1994). Moho and lower crustal reflectivity beneath a young rift basin: Results from a two-ship, wide-aperture seismic-reflection experiment in the Valencia trough (western Mediterranean). *Geophysical Journal International*, 118(1), 159–180. <https://doi.org/10.1111/j.1365-246x.1994.tb04681.x>
- Lanaja, M. (Ed.) (1987). *Contribución de la exploración petrolífera al conocimiento de la geología de España* (p. 465). Instituto Geológico y Minero de España.
- Maillard, A., Mauffret, A., Watts, A. B., Torné, M., Pascal, G., Buhl, P., & Pinet, B. (1992). Tertiary sedimentary history and structure of the Valencia trough (western Mediterranean). *Tectonophysics*, 203(1–4), 57–75. [https://doi.org/10.1016/0040-1951\(92\)90215-r](https://doi.org/10.1016/0040-1951(92)90215-r)
- Pascal, G., Torné, M., Buhl, P., Watts, A. B., & Mauffret, A. (1992). Crustal and velocity structure of the Valencia trough (western Mediterranean) Part II: Detailed interpretation of 5 expanded Spread profiles. *Tectonophysics*, 203(1–4), 21–35. [https://doi.org/10.1016/0040-1951\(92\)90213-p](https://doi.org/10.1016/0040-1951(92)90213-p)
- Shipboard Scientific Party. (1970). Western Alboran basin - Site 121. In W. B. F. Ryan & K. J. Hsu (Eds.), *Initial reports of the deep sea drilling project* (pp. 43–89). U.S. Government Printing Office.
- Stoffa, P., & Buhl, P. (1980). Two-ship multichannel seismic experiments for deep crustal studies. *Journal of Geophysical Research*, 84(B13), 7645–7660. <https://doi.org/10.1029/JB084iB13p07645>
- Taner, M. T., & Koehler, F. (1969). Velocity spectra-digital computer derivation and applications of velocity functions. *Geophysics*, 34(6), 859–881. <https://doi.org/10.1190/1.1440058>
- Torné, M., Pascal, G., Buhl, P., Watts, A. B., & Mauffret, A. (1992). Crustal and velocity structure of the Valencia trough (western Mediterranean) Part I: A combined refraction/wide angle reflection and near vertical reflection study. *Tectonophysics*, 203(1–4), 1–20. [https://doi.org/10.1016/0040-1951\(92\)90212-o](https://doi.org/10.1016/0040-1951(92)90212-o)
- Watts, A. B., & Mutter, J. (2015a). *Multi-Channel seismic shot data from the western Mediterranean Sea acquired during the R/V Robert D. Conrad expedition RC2911 (1988)*. IEDA. <https://doi.org/10.1594/IEDA/320898>
- Watts, A. B., & Mutter, J. (2015b). *Multi-Channel seismic shot data from the western Mediterranean Sea acquired during the R/V Robert D. Conrad expedition RC2911 (1988) with the R/V Jean Charcot participating*. IEDA. <https://doi.org/10.1594/IEDA/320902>